

vs. control subjects  $9.7\% \pm 2.1\%$  vs.  $8.1\% \pm 1.2\%$ ). The ratio of the lt S10 in COPD patients was significantly smaller than that in the controls ( $P < 0.05$ ) (COPD vs. control subjects  $3.9\% \pm 1.4\%$  vs.  $5.6\% \pm 2.4\%$ ).

## Discussion

The present study is the first to measure the volume of each pulmonary segment based on CT data and new software and to use this information to identify the differences between COPD patients and controls. We found that the upper lung volume of those with COPD is larger than in controls, although the lower lung volume of COPD patients is almost the same as in controls.

Worldwide, cigarette smoking is the most commonly encountered risk factor for COPD.<sup>1</sup> Pulmonary function tests often show findings of chronic airflow limitation in patients who have emphysema, and these patients are diagnosed as having COPD. In particular, centrilobular emphysema usually results from cigarette smoking and primarily involves the upper lung zones.<sup>14</sup> In this study, the volumes of pulmonary segments rt S2, lt S1+2, and lt S3 in COPD patients were significantly larger than those in the controls (Table 2). Soejima et al.<sup>8</sup> reported that longitudinally increasing changes in LAAs in smoking-induced damaged lungs were predominantly observed in the upper lung field. All of the COPD patients in the present study were either current or former smokers, and the results of this study support these facts. Furthermore, the volumes of pulmonary segments rt S5 and lt S5 in COPD patients were also significantly larger than those in the controls (Table 2). The pulmonary segments rt S5 and lt S5 in patients with COPD might have tendency to inflate compared with those of normal patients, caused by air trapping or emphysematous change itself. The middle lobe and lingular bronchi are easy to compress or obstruct, resulting in the collapse or atelectasis that has been called the middle lobe syndrome. This also might be reflected the phenomenon of decreasing volumes of pulmonary segments rt S5 and lt S5 in controls compared with those of COPD patients.

In general, physiological lung volume has diverse individual variation. In the present study, each pulmonary segmentation volume was divided by the total both-lung volume to revise individual variations. The volumes of pulmonary segments rt S2, rt S5, lt S1+2, lt S3, and lt S5 in COPD patients were significantly larger than those in the controls. However, in the volume of each pulmonary segment/total lung volume ratio, only two areas—rt S2 and lt S1+2—in COPD lungs were significantly greater than in the controls. As the height and weight of patients

with COPD did not differ from those of the controls, this result has two possible explanations: (1) both the volume of each pulmonary segment and the total lung volume increased; or (2) there was a relatively small number of COPD patients in this study.

Currently, researchers, particularly Japanese investigators, consider COPD to have two clinical phenotypes: an emphysema-dominant phenotype and an airway disease-dominant phenotype.<sup>15</sup> The airway disease-dominant phenotype is more common than the emphysema-dominant phenotype in women and in nonsmokers.<sup>15</sup> Clinical phenotypes of COPD have been classified according to the findings of high-resolution computed tomography (HRCT).<sup>16,17</sup> Comparing the volume of each pulmonary segment in two clinical phenotypes might be useful to elucidate the differences between the clinical phenotypes of COPD. Unfortunately, the number of COPD patients in the present study was insufficient to analyze the differences in clinical phenotypes.

There are some limitations of the present study. First, the software was assessed to have statistically good correlation between the result of the developer and that of the chest radiologist ( $P < 0.001$ ,  $r = 0.948$ ). However, as shown in Fig. 9, there were 32 cases that were outlying the range (y-axis: mean difference  $\pm 2$  SD) between the two data sets. This is because we used vessel-tracking software to extract the vessel-running data. Briefly, using vessel-tracking software, we determined the subsegmental vein forming each pulmonary segment ourselves, and thus determination of a false vessel would have resulted in an incorrect pulmonary segment border. Thus, the user must have sufficient knowledge of lung vessel running to determine the correct subsegmental veins. Therefore, we need to develop an algorithm that automatically tracks subsegmental veins, which would increase the accuracy of the software. Second, this software takes an hour to emphasize the lung lobe fissures using the sheet filter method and about 20 min to interpolate the fissures by the thin plate spline method. Thus, the algorithm needs to be improved to reduce the processing time and render it a useful clinical tool. Third, the number of COPD patients in this study was relatively small; and, finally, it was a retrospective study. A prospective study with a larger number of patients is required to confirm our results. However, the aim of this study was to measure each pulmonary segment's volume based on volumetric CT data using newly developed software and to identify the differences between COPD and controls, which we achieved. We believe that this software will be useful for elucidating the clinical character of COPD. In addition, the software could be applied to evaluate the process of lung volumes in various diffuse parenchymal lung diseases in the near future.

## Conclusion

The volumes of pulmonary segments based on volumetric CT data were measured using our newly developed three-dimensional software, and the differences between COPD and controls were identified. The volumes of the upper lobe segments in patients with COPD were larger than those in controls, whereas the volumes of the lower lobe segments in patients with COPD were almost the same as those in the controls.

## References

1. Global Initiative for Chronic Obstructive Lung Disease (GOLD). Global strategy for the diagnosis, management, and prevention of chronic obstructive pulmonary disease. Updated 2005.
2. Goddard PR, Nicholson EM, Laszlo G, Watt I. Computed tomography in pulmonary emphysema. *Clin Radiol* 1982;33: 379–87.
3. Bergin C, Müller N, Nichols DM, Lillington G, Hogg JC, Mullen B, et al. The diagnosis of emphysema: a computed tomographic–pathologic correlation. *Am Rev Respir Dis* 1986;133:541–6.
4. Gevenois PA, De Vuyst P, Sy M, Scillia P, Chaminade L, de Maertelaer V, et al. Pulmonary emphysema: quantitative CT during expiration. *Radiology* 1996;199:825–9.
5. Orlandi I, Moroni C, Camiciottoli G, Bartolucci M, Pistolesi M, Villari N, et al. Chronic obstructive pulmonary disease: thin-section CT measurement of airway wall thickness and lung attenuation. *Radiology* 2005;234:604–10.
6. Berger P, Perot V, Desbarats P, Tunon-de-Lara JM, Marthan R, Laurent F. Airway wall thickness in cigarette smokers: quantitative thin-section CT assessment. *Radiology* 2005;235: 1055–64.
7. Hasegawa M, Nasuhara Y, Onodera Y, Makita H, Nagai K, Fuke S, et al. Airflow limitation and airway dimensions in chronic obstructive pulmonary disease. *Am J Respir Crit Care Med* 2006;173:1309–15.
8. Soejima K, Yamaguchi K, Kohda E, Takeshita K, Ito Y, Mastubara H, et al. Longitudinal follow-up study of smoking-induced lung density changes by high-resolution computed tomography. *Am J Respir Crit Care Med* 2000;161:1264–73.
9. Committee of Pulmonary Physiology, Japanese Respiratory Society. Guidelines for pulmonary function tests: spirometry, flow-volume curve, diffusion capacity of the lung. Tokyo: Japanese Respiratory Society; 2004 (in Japanese).
10. Nishida S, Kambe M, Sewake N, Takano M, Kawane H. Pulmonary function in healthy subjects and its prediction. 5. Pulmonary diffusing capacity in adults. *Jpn J Clin Pathol* 1976;24:941–7.
11. Sato Y, Nakajima S, Shiraga N, Atsumi H, Yoshida S, Koller T, et al. Three-dimensional multi-scale line filter for segmentation and visualization of curvilinear structures in medical images. *Med Image Anal* 1998;2:143–68.
12. Bookstein FL. Principal warps: thin-plate splines and decomposition of deformations. *IEEE Trans Pattern Anal Mach Intell* 1989;11:567–85.
13. Boztosun I, Chara A, Zerroukat M, Djidjeli K. Thin-plate spline radial basis function scheme for advection-diffusion problems. *Electronic J Boundary Elements* 2002;2:267–82.
14. Thurlbeck WM, Simon G. Radiographic appearance of the chest in emphysema. *AJR Am J Roentgenol* 1978;130: 429–40.
15. Tatsumi K, Kasahara Y, Kurosu K, Tanabe N, Takiguchi Y, Kuriyama T. Respiratory Failure Research Group in Japan. Clinical phenotypes of COPD: results of a Japanese epidemiological survey. *Respirology* 2004;9:331–6.
16. Kitaguchi Y, Fujimoto K, Kubo K, Honda T. Characteristics of COPD phenotypes classified according to the findings of HRCT. *Respir Med* 2006;100:1742–52.
17. Fujimoto K, Kitaguchi Y, Kubo K, Honda T. Clinical analysis of chronic obstructive pulmonary disease phenotypes classified using high-resolution computed tomography. *Respirology* 2006;11:731–40.

## Nonspecific Interstitial Pneumonia Associated with Collagen Vascular Disease: Analysis of CT Features to Distinguish the Various Types

Tadahisa Daimon<sup>1</sup>, Takeshi Johkoh<sup>2</sup>, Osamu Honda<sup>3</sup>, Hiromitsu Sumikawa<sup>3</sup>, Kazuya Ichikado<sup>4</sup>, Yasuhiro Kondoh<sup>5</sup>, Hiroyuki Taniguchi<sup>5</sup>, Kiminori Fujimoto<sup>6</sup>, Masahiro Yanagawa<sup>3</sup>, Atsuo Inoue<sup>3</sup>, Noriyuki Tomiyama<sup>3</sup>, Hironobu Nakamura<sup>3</sup> and Yukihiro Sugiyama<sup>1</sup>

---

### Abstract

---

**Objective** The purpose of this study was to analyze the CT findings of interstitial lung diseases that are associated with collagen vascular disease (CVD), with particular attention to nonspecific interstitial pneumonia (NSIP), and to examine whether it is possible to predict the clinical diagnosis of CVDs based on the CT findings alone.

**Methods** CT scans of 49 patients with NSIP associated with CVD (15 males, 34 females; mean age, 55±10 years; age range, 25-76 years) were included in this retrospective study. All patients underwent a surgical biopsy. The clinical diagnosis comprised rheumatoid arthritis (RA) (n=15), systemic sclerosis (SSc) (n=8), polymyositis and dermatomyositis (PM/DM) (n=18), Sjögren's syndrome (SjS) (n=4), and mixed connective tissue disease (MCTD) (n=4). Each CT was reviewed by two independent observers who made a clinical diagnosis based on the CT findings alone.

**Results** The observers made a correct diagnosis for 22 (45%) of the 49 patients. A correct diagnosis was made for: RA in 7 (47%) of 15 patients; SSc in 3 (38%) of 8 patients; PM/DM in 11 (61%) of 18 patients; SjS in 1 (25%) of 4 patients. None of the 4 MCTD cases was diagnosed.

**Conclusion** It is difficult to make a correct clinical diagnosis of the various types of CVDs based solely on CT findings. However, it is probable to make a reasonably accurate clinical diagnosis in cases that show the typical CT findings, especially for PM/DM patients.

**Key words:** collagen vascular diseases, interstitial lung disease, computed tomography

(Inter Med 48: 753-761, 2009)

(DOI: 10.2169/internalmedicine.48.1714)

---

### Introduction

---

Collagen vascular diseases (CVDs) constitute a group of autoimmune disorders that can involve the respiratory system and cause focal or diffuse pulmonary disease. CVDs that show radiologic features of interstitial lung disease in-

clude rheumatoid arthritis (RA), systemic lupus erythematosus (SLE), systemic sclerosis (SSc), polymyositis and dermatomyositis (PM/DM), Sjögren's syndrome (SjS), and mixed connective tissue disease (MCTD). The American Thoracic Society and European Respiratory Society defined the following seven distinct types of idiopathic interstitial pneumonia (IIP): idiopathic pulmonary fibrosis (IPF) or

---

<sup>1</sup>Department of Medicine, Division of Pulmonary Medicine, Jichi Medical University, Shimotsuke, <sup>2</sup>Department of Radiology, Kinki Central Hospital, Itami, <sup>3</sup>Department of Radiology, Osaka University Graduate School of Medicine, Suita, <sup>4</sup>Department of Respiratory Medicine, Saiseikai Kumamoto Hospital, Kumamoto, <sup>5</sup>Department of Respiratory Medicine and Allergy, Tosei General Hospital, Seto and <sup>6</sup>Department of Radiology, Kurume University School of Medicine, Kurume

Received for publication September 25, 2008; Accepted for publication January 28, 2009

Correspondence to Dr. Tadahisa Daimon, tada0605@jichi.ac.jp

**Table 1. Demographic Data of Patients with NSIP Associated with CVD**

	RA (n=15)	SSc (n=8)	PM/DM (n=18)	SjS (n=4)	MCTD (n=4)	p values
Male / female	7 / 8	3 / 5	3 / 15	1 / 3	1 / 3	0.450
Age (year)	53.5 ± 7.7	56.6 ± 12.3	54.0 ± 11.6	54.8 ± 8.2	54.5 ± 7.8	0.999
Smoking index (pack-years)	15.5 ± 12.7	24.0 ± 15.0	10.2 ± 25.8	0	0	0.102
VC (L)	2.2 ± 0.6	2.1 ± 0.7	1.7 ± 0.4	2.0 ± 0.5	1.9 ± 0.2	0.315
VC (% predicted)	71.5 ± 14.0	71.1 ± 9.3	68.4 ± 14.3	75.5 ± 21.2	76.8 ± 3.1	0.750
FEV1 (L)	1.9 ± 0.5	1.9 ± 0.8	1.5 ± 0.4	1.7 ± 0.3	1.7 ± 0.3	0.490
FEV1/FVC (%)	86.7 ± 7.8	88.3 ± 2.5	86.2 ± 7.3	92.2 ± 6.4	89.8 ± 9.5	0.807

Note.-Data are shown as means ± SD. The data was assessed with the Kruskal-Wallis H-test.

Abbreviations: NSIP: nonspecific interstitial pneumonia, CVD: collagen vascular disease, RA: rheumatoid arthritis, SSc: systemic sclerosis, PM/DM: polymyositis and dermatomyositis, SjS: Sjögren's syndrome, MCTD: mixed connective tissue disease, VC: vital capacity, FEV1: forced expiratory volume in one second, FVC: forced vital capacity.

usual interstitial pneumonia (UIP), nonspecific interstitial pneumonia (NSIP), cryptogenic organizing pneumonia (COP) or bronchiolitis obliterans organizing pneumonia (BOOP), acute interstitial pneumonia, respiratory bronchiolitis-associated interstitial lung disease (RB-ILD), desquamative interstitial pneumonia (DIP), and lymphoid interstitial pneumonia (LIP) (1). At pathologic examination, interstitial lung diseases associated with CVD are diverse and include UIP, NSIP, COP (or BOOP), diffuse alveolar damage (DAD), and LIP (2).

Computed tomography (CT) is the most widely available, important, and standardized modality for the evaluation of interstitial lung diseases. The abnormal CT findings seen with IIPs and interstitial lung diseases associated with CVD have been extensively investigated.

Pathologic findings from patients with rheumatoid lung disease have revealed five different groups based on the specimens obtained at open lung biopsy: pulmonary rheumatoid nodules, UIP, BOOP, lymphoid hyperplasia, and NSIP (3). The CT findings reported in patients who have RA include bronchiectasis, bronchiolitis obliterans (i.e., air-trapping, mosaic perfusion), pleural effusions or pleural thickening, and enlarged lymph nodes (4).

Interstitial lung diseases associated with SLE are uncommon; in one series of 120 patients, only five (4%) had findings of interstitial lung diseases (5). The CT findings of interstitial fibrosis with SSc are similar to those of idiopathic NSIP and less extensive, less coarse, and characterized by a greater proportion of ground-glass attenuation than seen in patients with IPF (6). The types of interstitial lung diseases associated with PM/DM were identified, as follows, based on pathologic patterns: NSIP, UIP or BOOP, and DAD (7). A relatively high prevalence of consolidation (52%) and a low prevalence of honeycombing (16%) which is lower than in patients with SSc (8), were observed on high-resolution CT (HRCT) findings (9).

The common CT findings in SjS consisted of bronchiectasis and poorly defined centrilobular nodular or branching linear opacities, areas with ground-glass attenuation, and honeycombing (10). LIP frequently occurs in association with SjS, a characteristic pattern of extensive areas with ground-glass attenuation with scattered thin-walled cysts is seen in approximately 50% of LIP patients (11). The predominant abnormalities in MCTD included ground-glass attenuation, subpleural micronodules, and nonseptal linear

opacities (12). The frequency of honeycombing in MCTD was lower than in SSc and higher than in PM/DM (8).

The most common type of interstitial lung disease associated with CVD is NSIP (2), followed by UIP (2). The purpose of this study was to analyze the CT findings of interstitial lung diseases associated with CVD, with particular attention to NSIP, and to examine whether it is possible to determine the clinical diagnosis of CVDs based on the CT findings alone, with particular attention to the five common CVDs, namely RA, SSc, PM/DM, SjS, and MCTD.

## Methods

### Study population

CT scans of 66 patients with interstitial lung diseases associated with CVD, taken between January 1995 and December 2006 at four institutions, were collected for this retrospective study. Ultimately, 49 patients with NSIP associated with CVD were enrolled. Demographic data of patients with NSIP associated with CVD are summarized in Table 1. The patients included 15 males and 34 females, aged 55±10 years (mean ± SD) (range: 25-76 years). The institutional review board gave full approval and waived informed consent for this retrospective study.

All patients underwent open lung biopsy or video-assisted thoracoscopic surgery (VATS) and all interstitial lung diseases were histologically proved at each participating institution. Biopsy specimens were obtained from 2 to 3 different lobes in each patient. The diagnosis of interstitial lung disease was based on the current histologic criteria for the diagnosis of the relevant disease by at least two experienced chest pathologists (with more than 15 years experience) (1). The clinical findings of all cases, including those from the CT, were subsequently reviewed by chest physicians. Thus, patients with infectious diseases or other types of interstitial pneumonia associated with pneumoconiosis, eosinophilic lung diseases or hypersensitivity pneumonitis were excluded. The pathological diagnoses of interstitial lung disease comprised UIP (n=12), NSIP (n=49), OP (n=1), DAD (n=2), and LIP (n=2). The clinical diagnoses of CVD with NSIP comprised RA (n=15), SSc (n=8), PM/DM (n=18), SjS (n=4), and MCTD (n=4). All four patients with SjS had primary Sjögren's syndrome.

### **Thin-section CT techniques**

Sequential CT scans were obtained using a variety of scanners. All CT scans were performed at the end of inspiration with the patient in the supine position, and no intravenous contrast material was used. Each patient had a single chest CT examination. The CT scans consisted of 1- to 2-mm collimation sections reconstructed using a high-spatial-frequency algorithm. Images were photographed at window settings appropriate for viewing both the lung (window level from -600 to -800 HU; window width from 1,200 to 2,000 HU) and the mediastinal (window level from 20 to 80 HU; window width from 300 to 400 HU) windows. The protocols consisted of thin-sections obtained at 1-cm intervals (40 patients), 2-cm intervals (7 patients), or 3-cm intervals (2 patients).

### **Evaluation of thin-section CT findings**

The CT scans were randomized and then retrospectively reviewed by two independent chest radiologists (O.H., H.S.). The observers knew that they were all NSIP cases associated with CVD; they were also aware of the patient's age and gender, but were unaware of any other clinical findings. The CT scans were assessed for the presence and extent of areas with ground-glass attenuation, areas of air-space consolidation, honeycombing, cysts, intralobular reticular opacity, nonseptal linear or platelike opacity, subpleural lines, thickening of bronchovascular bundles, interlobular septal thickening, centrilobular nodules, traction bronchiectasis, pleural thickening, pleural effusion, pericardial effusion, and lymph node enlargement.

Ground-glass attenuation was defined as hazy increased attenuation of the lung that did not obscure the underlying vessels (13, 14). Air-space consolidation was defined as a homogeneous increase in pulmonary parenchymal attenuation that obscured the underlying vessels (13, 14). Honeycombing was considered present when clustered cystic airspaces that ranged in size from 2 mm to 1 cm with well-defined thick walls were seen in the subpleural regions (13, 14). Cysts were defined as round airspaces with a well-defined wall (13, 14). Intralobular reticular opacity was considered present when interlacing line shadows were separated by a few millimeters (13, 14). Nonseptal linear or platelike opacity was defined as an elongated line of soft-tissue attenuation that was distinct from interlobular septa and bronchovascular bundles (13, 14). Subpleural lines were defined as a curvilinear opacity a few millimeters or less in thickness, less than 1 cm from the pleural surface and paralleling pleura (13, 14). Thickening of bronchovascular bundles was defined as an increase in bronchial wall thickness and an increase in the diameter of pulmonary artery branches caused by thickened peribronchovascular interstitium (13). Interlobular septal thickening was defined as abnormal widening of interlobular septa (13, 14). A nodule was defined as a focal, rounded opacity of less than 3 cm in diameter, which could be either well or poorly defined.

When a nodule was located in the center of the lobule or lobular core, it was defined as a centrilobular nodule (13). Traction bronchiectasis was defined as irregular bronchial dilatation within or around areas with a parenchymal abnormality. Architectural distortion was considered present when bronchi, pulmonary vessels, or interlobar fissures or septa were abnormally displaced (14). Lymph nodes were considered to be enlarged if their short-axis diameter on CT exceeded 10 mm.

The lungs were divided into six zones (upper, middle, and lower zones in both lungs), and each zone was evaluated separately. The upper zone was defined as the part of the lung above the level of the tracheal carina; the lower zone, as the part of the lung below the level of the inferior pulmonary vein; and the middle zone, as the portion of the lung between the upper and lower zones. Each CT finding was assessed and considered present, and the extent of involvement of the findings was evaluated visually and independently for each lung zone. A score was assigned on the basis of the percentage of lung parenchyma that showed evidence of an abnormality and was estimated to the nearest 10% of parenchymal involvement. The overall percentage of involvement was calculated by averaging the scores of the six lung zones.

The extent of traction bronchiectasis was evaluated by counting the number of segments that showed evidence of traction bronchiectasis. The following 18 segments or sub-segments were evaluated: right apical upper, right anterior upper, right posterior upper, right lateral middle, right medial middle, right superior upper, right medial basal, right anterior basal, right lateral basal, right posterior basal, left apicoposterior upper, left anterior upper, left superior lingular, left inferior lingular, left superior lower, left anteromedial basal, left lateral basal, and left posterior basal. The extent of traction bronchiectasis was also quantified by assessing the generations of the most proximal bronchial branches involved. Traction bronchiectasis was scored as follows: 0, no bronchial dilatation; 1, bronchial dilatation involving bronchi distal to the fourth-generation bronchi; 2, bronchial dilatation involving from the second- and third-generation bronchi; 3, bronchial dilatation involving the trachea and/or the main bronchus.

After assessing the presence and extent of findings, the observers evaluated their predominant distribution. Zonal predominance was assessed as being upper or lower. Upper lung zone predominance was present when most of the abnormalities were above the level of the tracheal carina; and lower zone predominance was present when most of the abnormalities were below this level. The anatomic distribution was noted to be central if the abnormalities were primarily located in the inner third of the lung, and peripheral if the abnormalities were primarily present in the outer third of the lung. Peribronchovascular predominance was defined as findings located mainly around the bronchus and artery.

After reviewing the thin-section CT findings, the observers recorded the clinical diagnosis of CVDs, as suggested by

**Table 2. Summary of CT Findings of Each Interstitial Lung Diseases Associated with CVD**

Diagnosis	CT findings
RA	Intralobular reticular opacity, honeycombing, lower lung zone and posterior predominance. Bronchiectasis, centrilobular nodules. Pleural effusions or pleural thickening, and enlarged lymph nodes.
SSc	Intralobular reticular opacity similar to those of idiopathic NSIP and less extensive, less coarse. Ground-glass attenuation, air-space consolidation, lower lung zone and posterior predominance.
PM/DM	Air-space consolidation, a low prevalence of honeycombing (lower than SSc), lower lung zone and posterior predominance. Nonseptal linear or platelike, subpleural lines.
SjS	Bronchiectasis, centrilobular nodules, thickening of bronchovascular bundles. Ground-glass attenuation with scattered thin-walled cysts.
MCTD	A combination of those seen in SLE, SSc, and PM/DM. Ground-glass attenuation, air-space consolidation, honeycombing (lower than SSc and higher than PM/DM). Pleural effusions or pleural thickening.

Note. The descriptions of CT findings are based on information from references 3-15.

Abbreviations: CT: computed tomography, CVD: collagen vascular disease, RA: rheumatoid arthritis, SSc: systemic sclerosis, PM/DM: polymyositis and dermatomyositis, SjS: Sjögren's syndrome, MCTD: mixed connective tissue disease.

the CT findings according to previously published data of each interstitial lung diseases associated with CVD (Table 2). Differential diagnosis was limited to the five types (RA, SSc, PM/DM, SjS, and MCTD).

**Statistical analysis**

All statistical analyses were performed using statistical software (SPSS, version 12.0J; SPSS, Tokyo, Japan). The inter-observer variation for the extent of various abnormalities was analyzed using the Bland-Altman plot. The inter-observer variation for the clinical diagnosis of CVDs based on CT findings was analyzed with the  $\kappa$  statistic. Inter-observer agreement was classified as poor ( $\kappa=0.00-0.20$ ), fair ( $\kappa=0.21-0.40$ ), moderate ( $\kappa=0.41-0.60$ ), good ( $\kappa=0.61-0.80$ ), or excellent ( $\kappa=0.81-1.00$ ). Statistical significance was defined as  $p<0.05$ .

The readings of the two observers pertaining to the extent of various abnormal findings were combined by calculating the average. Disagreement regarding the existence of pleural thickening, pleural effusion, pericardial effusion, lymph node enlargement, the anatomic distribution, the zonal predominance, and the clinical diagnosis of CVDs based on the CT findings was resolved by the consensus of the two observers.

The Kruskal-Wallis *H*-test was used to evaluate differences in the demographic data of patients, the extent of various abnormalities, pleural thickening, pleural effusion, pericardial effusion, lymph node enlargement, the anatomic distribution, and the zonal predominance between each NSIP associated with CVD. A post-hoc test (Tukey's HSD procedure) was used to evaluate differences between each set of two groups.

**Results**

**Observer agreement**

Inter-observer agreement for the clinical diagnosis of CVDs based on CT findings was fair ( $\kappa=0.28$ ).

The result of the Bland-Altman plot between the two observers is shown in Fig. 1. The x-axis of this graph is the average of two results for the extent of various abnormali-

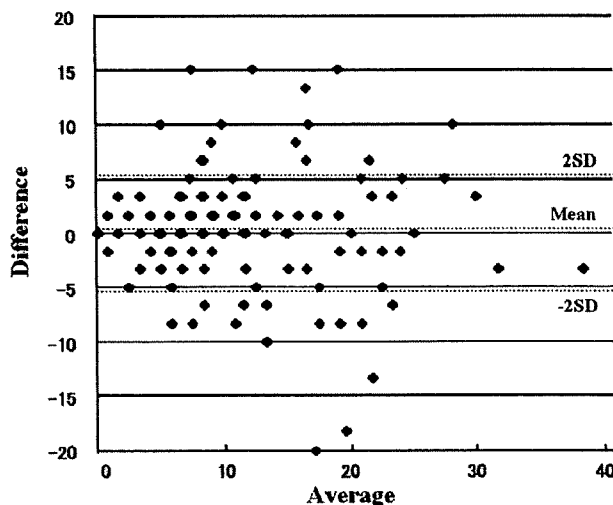


**Figure 1. Bland-Altman plot of the extent of various abnormalities. This graph was plotted to compare two results of the extent of various abnormalities (Horizontal axis: the average of two results, Vertical axis: the difference of two results).**

ties. The y-axis represents the difference between two results for the extent of various abnormalities. This assay indicates the inter-observer agreement of the extent of various abnormalities, if each plot existed within the bound of the average  $\pm 2 \times$  SD of difference of two results. The SD was 2.6 (2 SD=5.2), and the average was 0.3 (%) (Fig. 1).

**Diagnosis**

The observers made a correct diagnosis for 22 (45%) of the 49 patients, as summarized in Table 3. A correct diagnosis of RA was made for 7 (47%) of 15 patients (Figs. 2-4); of the 8 RA cases misdiagnosed by the observer, 3 were incorrectly recorded as SSc and 5 as PM/DM. A correct diagnosis of SSc was made for 3 (38%) of 8 patients (Figs. 5-7); of the 5 misdiagnosed SSc cases, the observer recorded 4 as RA and 1 as PM/DM. A correct diagnosis of PM/DM was made for 11 (61%) of 18 patients (Figs. 8, 9); of the 7 misdiagnosed PM/DM cases, the observer recorded 5 as RA and 2 as SSc. A correct diagnosis of SjS was made



**Figure 2.** Nonspecific interstitial pneumonia (NSIP) associated with RA in a 63-year-old man. Transverse thin-section CT (2-mm collimation) at the level of tracheal carina demonstrates areas of air-space consolidation with traction bronchiectasis (large arrows) in a predominantly peribronchovascular distribution, and extensive diffusely distributed centrilobular nodules (small arrows).

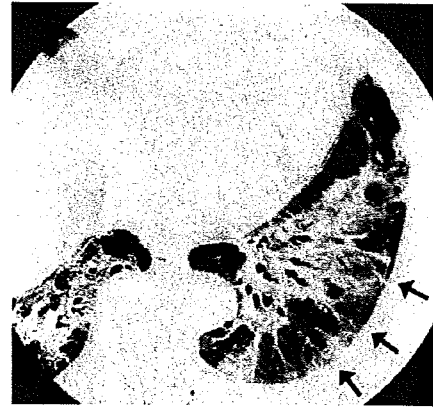


**Figure 4.** Nonspecific interstitial pneumonia (NSIP) associated with RA in a 55-year-old woman. Transverse thin-section CT (2-mm collimation) through the left lower lobe demonstrates areas of air-space consolidation (arrows) with a predominantly peribronchovascular distribution.



**Figure 3.** Nonspecific interstitial pneumonia (NSIP) associated with RA in a 54-year-old man. Transverse thin-section CT (1-mm collimation) at the level of the right inferior pulmonary vein demonstrates intralobular reticular opacity (arrows) with a predominantly peripheral distribution.

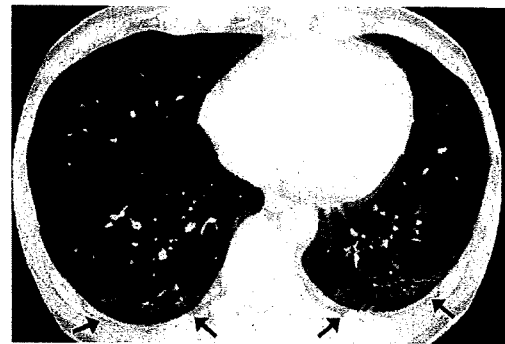


**Figure 5.** Nonspecific interstitial pneumonia (NSIP) associated with SSc in a 42-year-old man. Transverse thin-section CT (1-mm collimation) through the lower lobes demonstrates intralobular reticular opacity (arrows) with a predominantly peripheral distribution.

for 1 (25%) of 4 patients (Fig. 10). None of the 4 MCTD cases was diagnosed based on CT findings alone (Fig. 11).

#### **Extent and distribution of CT findings**

Significant differences in the extent of various abnormalities between each patient with NSIP associated with CVD were found with honeycombing ( $p=0.014$ ), cysts ( $p=0.030$ ), intralobular reticular opacity ( $p=0.007$ ), subpleural lines ( $p=0.002$ ), and interlobular septal thickening ( $p=0.042$ ) (Table 4).

Among patients with NSIP associated with CVD, areas with ground-glass attenuation were present in all types of



**Figure 6.** Nonspecific interstitial pneumonia (NSIP) associated with SSc in a 52-year-old woman. Transverse thin-section CT (2-mm collimation) at the level of the right superior pulmonary vein demonstrates areas of air-space consolidation (arrows) with a predominantly peripheral distribution.



**Figure 7.** Nonspecific interstitial pneumonia (NSIP) associated with SSc in a 67-year-old woman. Transverse thin-section CT (1-mm collimation) at the level of the right inferior pulmonary vein demonstrates intralobular reticular opacity (large arrows) with predominantly peribronchovascular distribution and extensive diffusely distributed centrilobular nodules (small arrows).



**Figure 9.** Nonspecific interstitial pneumonia (NSIP) associated with PM/DM in a 51-year old woman. Transverse thin-section CT (2-mm collimation) through the left lower lobe demonstrates intralobular reticular opacity (large arrows) with a predominantly peripheral distribution and platelike opacity (small arrow).

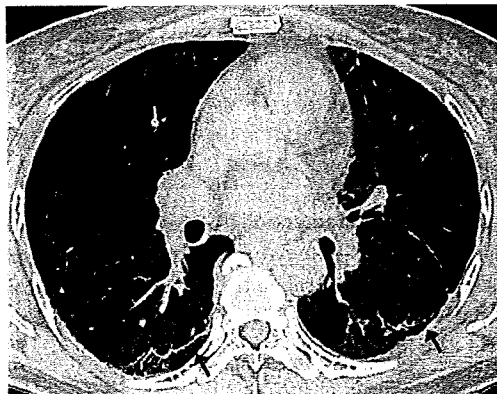


**Figure 8.** Nonspecific interstitial pneumonia (NSIP) associated with polymyositis and dermatomyositis (PM/DM) in a 51-year-old woman. Transverse thin-section CT (2-mm collimation) at the level of the inferior pulmonary vein demonstrates subpleural lines (arrows).



**Figure 10.** Nonspecific interstitial pneumonia (NSIP) associated with SjS in a 62-year old woman. Transverse thin-section CT (1-mm collimation) at the level of the inferior pulmonary vein demonstrates intralobular reticular opacity with traction bronchiectasis (arrows) with a predominantly peribronchovascular distribution.

CVDs and showed the greater extent in SSc, although the differences were not significant ( $p=0.369$ ). Areas of air-space consolidation were found in all types of CVDs with similar extent, except for MCTD in which this finding showed the lowest extent. Honeycombing was present in four types of CVDs, except for SjS. The extent of honeycombing in MCTD was significantly greater than those in SSc ( $p=0.050$ ). The extent of honeycombing in SSc was less than in RA and PM/DM, but there were no significant differences ( $p=0.853, 0.895$ ). Cysts were present in PM/DM, SjS, and MCTD with similar extent. Intralobular reticular opacity was present in all types of CVDs. The extent of in-

tralobular reticular opacity in SSc was significantly greater than in RA ( $p=0.007$ ) and PM/DM ( $p=0.029$ ) (Fig. 5). Non-septal linear or platelike opacity was present in all types of CVDs, but with no significant differences ( $p=0.701$ ). Subpleural lines were found in all types. The extent of subpleural lines in PM/DM was significantly greater than those in RA ( $p=0.024$ ) and SSc ( $p=0.017$ ) (Fig. 8). The extent of subpleural lines in MCTD was also greater than others, but there were no significant differences (Fig. 11). Interlobular



septal thickening was found in all types. The extent of interlobular septal thickening in SjS was significantly greater than in RA ( $p=0.050$ ). Centrilobular nodules were present in RA, SSc, and PM/DM, and showed a greater extent in RA (Fig. 2), although the differences were not significant. Traction bronchiectasis was present in all types, but with no significant difference.

Pleural thickening and lymph node enlargement were present in all types, and the differences were not significant. Pleural effusion was present in SSc, PM/DM, and SjS, with no significant differences. Pericardial effusion was absent in all types (Table 4).

The incidence of patients with RA and SjS with a lower zonal predominance was less than for the other 3 types ( $p=0.001$ ) (Table 4). There were no significant differences in anatomic distribution among patients with NSIP associated with CVD.

### Discussion

The observers made a correct diagnosis for 22 (45%) of the 49 patients. A correct diagnosis was made for: RA in 7 (47%) of 15 patients; SSc in 3 (38%) of 8 patients; PM/DM in 11 (61%) of 18 patients; and SjS in 1 (25%) of 4 patients. None of the 4 MCTD cases was diagnosed based on



**Figure 11.** Nonspecific interstitial pneumonia (NSIP) associated with mixed connective tissue disease (MCTD) in a 45-year-old woman. Transverse thin-section CT (1-mm collimation) at the level of the right inferior pulmonary vein demonstrates intralobular reticular opacity (large arrows) with a predominantly peripheral distribution and subpleural lines (small arrows).

CT findings alone.

The types of interstitial lung diseases associated with PM/DM were identified on the basis of pathologic patterns: NSIP, UIP or BOOP, and DAD (7). The frequency of honeycombing was 16% of patients who had abnormal HRCT findings (9), which is lower than in patients with SSc (8). In the present study, the extent of honeycombing in patients with NSIP with PM/DM was not significantly different from each other (Table 4). The extent of intralobular reticular opacity was less than in patients with NSIP with SSc, while it was also almost the same as in patients with NSIP with RA (Table 4). Nonseptal linear or plate-like opacity has been reported as one of the most common CT findings in interstitial lung diseases associated with PM/DM (9, 15). In the present study, in patients with NSIP with PM/DM, nonseptal linear or plate-like opacity was present in 7 (39%) of 18 patients (Fig. 9).

Subpleural lines were defined as a curvilinear opacity, which was also termed a subpleural curvilinear shadow, a few millimeters or less in thickness, less than 1 cm from the pleural surface and paralleling pleura (13, 14). It was first described in patients with asbestosis. This occurs as a result of atelectasis, fibrosis, or inflammation, and can be seen in a variety of lung diseases including IPF or UIP (16), as well as in normal patients as a result of atelectasis. Schurawitzki et al reported that 17 (74%) of 23 patients with SSc showed subpleural lines on HRCT (17). Mino et al reported that 7 (38%) of 19 patients with PM/DM showed subpleural lines on HRCT (18). In the present study, subpleural lines were present in: 12 (67%) of 18 NSIP cases with PM/DM; 4 (27%) of 15 NSIP cases with RA; 2 (15%) of 8 NSIP cases with SSc; 1 (25%) of 4 NSIP cases with SjS; and 2 (50%) of 4 NSIP cases with MCTD. Subpleural lines were therefore most commonly found in patients with NSIP with PM/DM (Fig. 8). This information may be useful in the diagnosis of interstitial lung diseases associated with PM/DM.

Pulmonary parenchymal abnormalities are more common and more severe in SSc than in the other types of CVD. The pathologic features are of NSIP or UIP, the former being more common (7). The CT findings of interstitial fibrosis with SSc are similar to those of idiopathic NSIP and less extensive, less coarse, and characterized by a greater proportion of ground-glass attenuation than seen in patients with IPF (6). In the present study, in NSIP patients with SSc, the extent of intralobular reticular opacity was significantly greater than those in RA ( $p=0.007$ ) and PM/DM ( $p=0.029$ ) (Table 4). The abnormalities showed lower lung zone and posterior predominance, which is the same as in a previous report (6) (Figs. 5, 6). This might be useful information for

**Table 3.** Clinical Diagnosis of NSIP Associated with CVD Based on CT Findings

	RA (n=15)	SSc (n=8)	PM/DM (n=18)	SjS (n=4)	MCTD (n=4)	Total (n=49)
Number (%)	7 (47)	3 (38)	11 (61)	1 (25)	0 (0)	22 (45)

Note. Data in parentheses are percentages.

Abbreviations: NSIP: nonspecific interstitial pneumonia, CVD: collagen vascular disease, CT: computed tomography, RA: rheumatoid arthritis, SSc: systemic sclerosis, PM/DM: polymyositis and dermatomyositis, SjS: Sjögren's syndrome, MCTD: mixed connective tissue disease.

**Table 4. Extent and Distribution of Thin-section CT Findings of Each NSIP Associated with CVD**

CT finding	RA (n=15) Extent	SSc (n=8) Extent	PM/DM (n=18) Extent	SjS (n=4) Extent	MCTD (n=4) Extent	p values
Ground-glass attenuation <sup>†</sup>	14.2 ± 9.0	17.4 ± 7.2	15.1 ± 7.8	11.5 ± 3.5	16.3 ± 13.5	0.369
Air-space consolidation <sup>†</sup>	7.7 ± 6.8	6.0 ± 6.2	5.2 ± 4.1	7.3 ± 4.4	2.1 ± 2.5	0.157
Honeycombing <sup>†</sup>	1.4 ± 3.1	0.2 ± 0.8 <sup>‡</sup>	1.3 ± 4.7	0	4.8 ± 4.1 <sup>‡</sup>	0.014 <sup>§</sup>
Cysts <sup>†</sup>	0 <sup>‡</sup>	0	0.4 ± 1.2	0.4 ± 0.7	1.0 ± 1.7 <sup>‡</sup>	0.030 <sup>§</sup>
Intralobular reticular opacity <sup>†</sup>	3.3 ± 6.0	9.8 ± 5.4 <sup>‡</sup>	4.4 ± 3.9 <sup>‡</sup>	2.9 ± 2.5	5.8 ± 7.2	0.007 <sup>§</sup>
Nonseptal linear or platelike opacity <sup>†</sup>	1.4 ± 2.3	1.0 ± 2.1	1.6 ± 2.1	1.5 ± 2.4	1.9 ± 2.2	0.701
Subpleural lines <sup>†</sup>	0.9 ± 2.0	1.2 ± 2.2 <sup>‡</sup>	2.7 ± 2.1 <sup>‡</sup>	1.4 ± 2.4	2.9 ± 2.5	0.002 <sup>§</sup>
Thickening of bronchovascular bundles <sup>†</sup>	0.2 ± 0.8	0.4 ± 1.1	0.3 ± 0.9	0	0.4 ± 1.1	0.222
Interlobular septal thickening <sup>†</sup>	0.2 ± 0.7	1.5 ± 3.2	0.6 ± 1.4	2.3 ± 2.0 <sup>‡</sup>	1.0 ± 1.7	0.042 <sup>§</sup>
Centrilobular nodules <sup>†</sup>	1.4 ± 3.1	0.6 ± 1.4	0.1 ± 0.4	0	0	0.189
Generations of traction bronchiectasis <sup>†</sup>	1.5 ± 0.5	1.3 ± 0.5	1.3 ± 0.5	1.3 ± 0.5	1.0 ± 0	0.075
No. of segments with traction bronchiectasis	10.8 ± 3.8	11.4 ± 3.2	9.9 ± 3.0	8.8 ± 4.5	11.0 ± 4.8	0.206
No. of patients with pleural thickening <sup>‡</sup>	3 (20)	4 (50)	9 (50)	1 (25)	2 (50)	0.181
No. of patients with pleural effusion <sup>‡</sup>	0 (0)	2 (25)	3 (17)	1 (25)	0 (0)	0.159
No. of patients with pericardial effusion <sup>‡</sup>	0 (0)	0 (0)	0 (0)	0 (0)	0 (0)	NA
No. of patients with lymph node enlargement <sup>‡</sup>	4 (27)	2 (25)	2 (11)	1 (25)	1 (25)	0.505
Zonal predominance						
No. of patients with upper predominance <sup>‡</sup>	3 (20)	1 (13)	0 (0)	1 (25)	0 (0)	0.062
No. of patients with lower predominance <sup>‡</sup>	10 (67) <sup>‡</sup>	7 (88)	17 (94)	2 (50)	4 (100) <sup>‡</sup>	0.001 <sup>§</sup>
Anatomic distribution						
No. of patients with central predominance <sup>‡</sup>	0 (0)	0 (0)	0 (0)	0 (0)	0 (0)	NA
No. of patients with peripheral predominance <sup>‡</sup>	8 (53)	3 (38)	9 (50)	2 (50)	3 (75)	0.850
No. of patients with peribronchovascular predominance <sup>‡</sup>	13 (87)	7 (88)	17 (94)	3 (75)	4 (100)	0.230

Note. †Unless otherwise indicated, data are mean ± standard deviation. The data was assessed with the Kruskal–Wallis H-test. NA = not available

<sup>‡</sup>Data are percentage of lung parenchyma.

<sup>†</sup>Data are scores.

<sup>‡</sup>Data in parentheses are percentages.

identifying interstitial lung diseases associated with SSc. However, there were some SSc cases with combined centrilobular nodules that the observers incorrectly recorded as RA (Fig. 7). It is difficult to clearly distinguish the clinical diagnosis of SSc from the other types based solely on CT findings.

In NSIP patients with RA, the extent of honeycombing was not significantly different from each other (Table 4). The extent of intralobular reticular opacity in RA was significantly less than those in SSc ( $p=0.007$ ). The extent of centrilobular nodules in RA was not significantly different from each other (Table 4). In the present study, pleural effusion was not present in patients with NSIP with RA. Pleural thickening was present in 3 (20%) of 15 RA patients with NSIP. Lymph node enlargement was present in 4 patients (27%). Patterns of CT findings from NSIP cases with RA were diverse (Figs. 2-4) and there were no characteristic CT findings of NSIP with RA to allow differentiation from the other 4 types with NSIP.

Sjögren's syndrome can occur as a primary disease, without features of other CVD, or as a secondary disease in association with other CVDs, most commonly RA. LIP frequently occurs in association with SjS, followed in frequency by airway abnormalities such as follicular bronchitis, bronchiectasis, and bronchiolitis (7). A characteristic pattern of extensive areas with ground-glass attenuation with scattered thin-walled cysts is seen in approximately 50% of pa-

tients with LIP (19). Poorly defined centrilobular nodules and thickening of the bronchovascular bundles, also seen in LIP, represent expansion of the interstitial tissue by lymphoplasmic cell infiltration (19). In the present study, cysts were seen in NSIP patients with SjS, but the extent of cysts was not significantly different from each other (Table 4). Honeycombing, thickening of bronchovascular bundles and centrilobular nodules were not seen in NSIP patients with SjS (Table 4).

Based on the findings of this study and previous reports (8, 12), CT findings of NSIP associated with MCTD resemble NSIP with PM/DM (Fig. 11). Saito et al (8) also concluded that CT findings in MCTD were a combination of those seen in other patients (SLE, SSc, and PM/DM). In the present study, 4 MCTD cases were recorded incorrectly as RA ( $n=2$ ), SSc ( $n=1$ ), and PM/DM ( $n=1$ ). Indeed, it is difficult to define the clinical diagnosis of MCTD based on the CT findings alone.

The present study has several limitations. First, the number of patients with NSIP associated with SjS and MCTD was relatively small. Second, patients with interstitial lung diseases associated with SLE were not included. Interstitial lung diseases associated with SLE are rare, and this limitation must be reflected in clinical practice. Third, this was a retrospective study and thus a prospective study is required to confirm the results. Finally, the CT images used in this study were obtained using different CT scanners and proto-

cols, and thus the details of each finding could be evaluated only to a limited degree.

In conclusion, generally speaking, it is difficult to arrive at a correct clinical diagnosis of CVDs based on CT findings alone. However, it is probable to make a reasonably accurate clinical diagnosis in cases that show the typical CT findings, especially for PM/DM patients. Using the detailed

findings on HRCT, a feasible method to predict the diagnosis of NSIP-associated CVD.

#### Acknowledgement

This study was supported by the Health and Labor Sciences Research Grants on Diffuse Lung Diseases from the Japanese Ministry of Health, Labor and Welfare.

### References

1. American Thoracic Society, European Respiratory Society. American Thoracic Society/European Respiratory Society International Multidisciplinary Consensus Classification of the Idiopathic Interstitial Pneumonias: this joint statement of the American Thoracic Society (ATS), and the European Respiratory Society (ERS) was adopted by the ATS Board of Directors, June 2001 and by the ERS Executive Committee, June 2001. *Am J Respir Crit Care Med* **165**: 277-304, 2002.
2. Tansey D, Wells AU, Colby TV, et al. Variations in histological patterns of interstitial pneumonia between connective tissue disorders and their relationship to prognosis. *Histopathology* **44**: 585-596, 2004.
3. Yousem SA, Colby TV, Carrington CB. Lung biopsy in rheumatoid arthritis. *Am Rev Respir Dis* **131**: 770-777, 1985.
4. Remy-Jardin M, Remy J, Cortet B, Mauri F, Delcambre B. Lung changes in rheumatoid arthritis: CT findings. *Radiology* **193**: 375-382, 1994.
5. Haupt HM, Moore GW, Hutchins GM. The lung in systemic lupus erythematosus: analysis of the pathologic changes in 120 patients. *Am J Med* **71**: 791-798, 1981.
6. Desai SR, Veeraraghavan S, Hansell DM, et al. CT features of lung disease in patients with systemic sclerosis: comparison with idiopathic pulmonary fibrosis and nonspecific interstitial pneumonia. *Radiology* **232**: 560-567, 2004.
7. Kim EA, Lee KS, Johkoh T, et al. Interstitial lung diseases associated with collagen vascular diseases: radiologic and histopathologic findings. *Radiographics* **22**: 151-165, 2002.
8. Saito Y, Terada M, Takada T, et al. Pulmonary involvement in mixed connective tissue disease: comparison with other collagen vascular diseases using high resolution CT. *J Comput Assist Tomogr* **26**: 349-357, 2002.
9. Ikezoe J, Johkoh T, Kohno N, Takeuchi N, Ichikado K, Nakamura H. High-resolution CT findings of lung disease in patients with polymyositis and dermatomyositis. *J Thorac Imaging* **11**: 250-259, 1996.
10. Franquet T, Gimenez A, Monill JM, Diaz C, Geli C. Primary Sjogren's syndrome and associated lung disease: CT findings in 50 patients. *AJR Am J Roentgenol* **169**: 655-658, 1997.
11. Koyama M, Johkoh T, Honda O, et al. Pulmonary involvement in primary Sjogren's syndrome: spectrum of pulmonary abnormalities and computed tomography findings in 60 patients. *J Thorac Imaging* **16**: 290-296, 2001.
12. Kozuka T, Johkoh T, Honda O, et al. Pulmonary involvement in mixed connective tissue disease: high-resolution CT findings in 41 patients. *J Thorac Imaging* **16**: 94-98, 2001.
13. Webb WR, Müller NL, Naidich DP. High-resolution computed tomography findings of lung disease. High-resolution CT of the lung. 3rd ed. Lippincott Williams & Wilkins, Philadelphia, 2001: 71-192.
14. Austin JH, Müller NL, Friedman PJ, et al. Glossary of terms for CT of the lungs: recommendations of the Nomenclature Committee of the Fleischner Society. *Radiology* **200**: 327-331, 1996.
15. Douglas WW, Tazelaar HD, Hartman TE, et al. Polymyositis-dermatomyositis-associated interstitial lung disease. *Am J Respir Crit Care Med* **164**: 1182-1185, 2001.
16. al-Jarad N, Strickland B, Pearson MC, Rubens MB, Rudd RM. High resolution computed tomographic assessment of asbestosis and cryptogenic fibrosing alveolitis: a comparative study. *Thorax* **47**: 645-650, 1992.
17. Schurawitzki H, Stiglbauer R, Graninger W, et al. Interstitial lung disease in progressive systemic sclerosis: high-resolution CT versus radiography. *Radiology* **176**: 755-759, 1990.
18. Mino M, Noma S, Taguchi Y, Tomii K, Kohri Y, Oida K. Pulmonary involvement in polymyositis and dermatomyositis: sequential evaluation with CT. *Am J Roentgenol* **169**: 83-87, 1997.
19. Johkoh T, Muller NL, Pickford HA, et al. Lymphocytic interstitial pneumonia: thin-section CT findings in 22 patients. *Radiology* **212**: 567-572, 1999.



# Interleukin-1 receptor-related protein ST2 suppresses the initial stage of bleomycin-induced lung injury

N. Mato\*, M. Fujii<sup>#</sup>, Y. Hakamata<sup>†</sup>, E. Kobayashi<sup>+</sup>, A. Sato<sup>§</sup>, M. Hayakawa<sup>#</sup>,  
H. Ohto-Ozaki<sup>#</sup>, M. Bando\*, S. Ohno\*, S. Tominaga<sup>#</sup> and Y. Sugiyama\*

**ABSTRACT:** Acute lung injury has a range of causes, and occasionally leads to lethal respiratory failure. Despite advances in treatment, acute lung injury continues to have a high mortality rate, and thus a new therapeutic approach is needed. ST2 is an interleukin (IL)-1 receptor-related protein, and its expression is induced by various inflammatory responses. Recently, ST2 has been speculated to exert anti-inflammatory effects; therefore, we investigated the role of the ST2 in the murine model of acute lung injury.

To elucidate the function of ST2 *in vivo*, mice that transiently overexpressed ST2 protein were prepared using the hydrodynamic gene transfer method, and lung injury was induced by intratracheal administration of bleomycin.

In bleomycin-treated ST2-overexpressing mice, the increase of neutrophils in the bronchoalveolar lavage fluid (BALF) was markedly suppressed. Additionally, the levels of tumour necrosis factor- $\alpha$  and IL-6, as well as the concentration of albumin, in BALF were reduced compared with those of controls. Furthermore, the pulmonary architecture in ST2-overexpressing mice remained almost normal, and the survival rate was significantly improved.

From these results, we concluded that ST2 has the potential to suppress the initial stage of acute lung injury, and therefore it may be a useful reagent for the treatment of acute lung injury.

**KEYWORDS:** Acute lung injury, bleomycin, hydrodynamic injection, ST2

**A**cute lung injury (ALI) can be triggered by various stimuli, including drugs, sepsis and trauma [1]. It is characterised by epithelial and endothelial damage, and is followed by destruction of the alveolar capillary-epithelial barrier. The increased permeability of pulmonary capillary vessels allows flooding of inflammatory cells, enables plasma proteins to enter the lung and results in a disturbance of gas exchange [1, 2]. The mortality rate of ALI patients remains high (40–60%) despite the numerous attempts that have been made to develop new therapies [2]. For the treatment of ALI, factors such as mechanical ventilation settings, oxygen concentration maintenance and the management of fluid balance have been extensively investigated, and new devices and techniques have led to important improvements. However, in spite of these efforts, an effective therapy to attenuate the inflammatory process in ALI has not been established.

TOMINAGA [3] originally identified the ST2 (interleukin (IL)-1 receptor-related) gene as an early-response gene in mouse fibroblasts. The ST2 gene generates at least four different gene products, the soluble secreted form (ST2), the transmembrane form (ST2L) and two variant forms (ST2V and ST2LV), by alternative splicing [4]. Recently, a specific ligand for ST2L was discovered and named IL-33 by SCHMITZ *et al.* [5]. ST2 has been known to be related to various disorders in humans and an increase of serum ST2 has been reported in conditions such as septic shock [6], severe trauma [6], bronchial asthma [7] and idiopathic pulmonary fibrosis, especially in acute exacerbation [8]. Several experimental studies have suggested that the induction of ST2 by various inflammatory stimuli may confer protection against inflammatory damage. For example, it has been reported that pre-treatment with ST2 resulted in an attenuation of pro-inflammatory cytokines and an enhanced survival rate in a

#### AFFILIATIONS

\*Division of Pulmonary Medicine, Dept of Medicine, Jichi Medical University,

<sup>#</sup>Dept of Biochemistry, Jichi Medical University,

<sup>+</sup>Division of Organ Replacement Research, Center for Molecular Medicine, Jichi Medical University, and,

<sup>§</sup>Dept of Dermatology, Jichi Medical University, Tochigi, and

<sup>†</sup>Dept of Basic Science, School of Veterinary Nursing and Technology, Nippon Veterinary and Life Science University, Musashino-shi, Japan.

#### CORRESPONDENCE

Y. Sugiyama

Division of Pulmonary Medicine, Jichi Medical University,

3311-1 Yakushiji,

Shimotsuke-Shi,

Tochigi 329-0498,

Japan.

Fax: 81 285443586

E-mail: sugiyuki@jichi.ac.jp

Received:

July 07 2007

Accepted after revision:

January 13 2009

#### SUPPORT STATEMENT

The present study was supported in part by a grant from the Center of Excellence in the 21st Century Program of the Ministry of Education, Culture, Sports, Science, and Technology of Japan (Tokyo, Japan).

#### STATEMENT OF INTEREST

None declared.

European Respiratory Journal

Print ISSN 0903-1936

Online ISSN 1399-3003

This article has supplementary material accessible from [www.erj.ersjournals.com](http://www.erj.ersjournals.com)

mouse endotoxin shock model [9]. ST2 has also been shown to inhibit degradation of inhibitor on nuclear factor- $\kappa$ B and suppress lipopolysaccharide-induced IL-6 production in THP-1 cells [10]. Additionally, in a collagen-induced arthritis model, it was demonstrated that ST2 suppressed the production of inflammatory cytokines and significantly attenuated the disease [11].

Taken together, these findings suggest that it is worthwhile to assess the therapeutic potential of ST2 as an anti-inflammatory agent *in vivo*. In the current study, ST2-overexpressing mice were prepared by the hydrodynamic gene transfer method, and the effects of ST2 on bleomycin-induced lung injury were investigated. Based on the anti-inflammatory effects of ST2, it was hypothesised that its *in vivo* overexpression would ameliorate bleomycin-induced lung injury in mice.

## MATERIALS AND METHODS

### Mice

Male C57BL/6 mice, aged 7–8 weeks (body weight 18–22 g), were purchased from Japan SLC (Hamamatsu, Japan). Mice were maintained under standard conditions and fed rodent chow and water *ad libitum*. The research proposal was reviewed by the animal ethical committee of Jichi Medical University (permission No. 152; Tochigi, Japan), and all experiments were performed in accordance with the Jichi Medical University Guide for Laboratory Animals, based on the Helsinki convention for the use and care of animals. The number of mice employed in the different experiments is described in the relevant figure legends.

### Plasmids

pCAGGS and pCAGGS-LacZ were kindly provided by J. Miyazaki (Osaka University, Osaka, Japan) and T. Murakami (Jichi Medical University, Tochigi, Japan), respectively. pCAGGS was an efficient expression vector driven by the chicken  $\beta$ -actin promoter, and pCAGGS-LacZ was constructed by insertion of the  $\beta$ -galactosidase reporter gene into pCAGGS. pCAGGS-mST2 was constructed by insertion of mouse ST2 (mST2) cDNA into the Xho1 restriction site of pCAGGS. The European Molecular Biology Laboratory/GeneBank accession number for the nucleotide sequence mST2 is Y07519. mST2 cDNA was originally isolated from the cDNA library of BALB/c-3T3 cells after growth stimulation with serum [12]. First, the Hinc 2 fragment of mST2 cDNA containing the entire coding region (1,582 bp) was inserted into the Xba1 site of the pEF-BOS plasmid (pEF-BOS-mST2) using an Xba1 linker. Secondly, the fragment of mST2 was obtained from pEF-BOS-mST2 by digestion with Xba1, and ligated with the Xho1 linker. Thirdly, the pCAGGS plasmid was digested with Xho1 and finally the mST2 fragment, digested with Xho1, was inserted. Plasmids were purified with a Plasmid Maxi Kit (Qiagen, Valencia, CA, USA). The pGL3 control vector containing a firefly luciferase reporter gene was purchased from Promega (Madison, WI, USA).

### Cell culture and in vitro transfection

To confirm that the constructed plasmid was appropriate for producing soluble recombinant ST2 protein, human embryonic kidney (HEK) 293T cells were cultured and transfected with pCAGGS and pCAGGS-mST2. HEK 293T cells were kindly provided by T. Kasahara (Kyoritsu University of Pharmacy,

Tokyo, Japan), and were cultured in Dulbecco's modified Eagle's medium (Sigma-Aldrich, St Louis, MO, USA) containing 10% (volume/volume (v/v)) foetal bovine serum (Thermo Trace, Melbourne, Australia). The amount of plasmid was 10  $\mu$ g, and transfection was carried out by the calcium phosphate precipitation method.

### Western blotting

20 h after the transfection of pCAGGS and pCAGGS-mST2, the culture medium was collected, digested with N-Glycosidase-F (Roche, Indianapolis, IN, USA), and subjected to sodium dodecyl sulphate-polyacrylamide gel electrophoresis and immunoblotting, as described previously [12]. In brief, proteins were separated electrophoretically with 10% polyacrylamide gel and transferred to an Immobilon-P membrane (Millipore, Bedford, MA, USA) at 100 mA for 1 h. Immunoblotting was performed with rabbit anti-mouse ST2 polyclonal antibody ( $\times 1000$  dilution) against the recombinant ST2 protein from *Escherichia coli*, and after incubation for 1 h at room temperature. Then the membrane was incubated for 0.5 h with anti-rabbit immunoglobulin (Ig) G-horseradish peroxidase (HRP;  $\times 5000$  dilution; Jackson ImmunoResearch, West Grove, PA, USA) as a secondary antibody, and the protein band was visualised by the ECL system (Amersham Bioscience, Amersham, UK).

### In vivo gene transfer

Plasmid vectors were delivered into mice by hydrodynamic injection, which is an efficient *in vivo* method of gene transfer. Plasmid DNA was diluted in sterile saline, and the final volume was adjusted to 6.3% of total body weight [13]. Under mild anesthesia with diethyl ether, mice were injected with the plasmid solution through the dorsal penile vein in 5–8 s, using a 26-gauge needle. The amount of plasmid vector was appropriately chosen in each experiment.

To evaluate liver damage, mice were sacrificed and blood was collected at 24 and 48 h after the hydrodynamic gene transfer. Serum aspartate aminotransferase (AST) and alanine aminotransferase (ALT) levels were assayed by the Japan Society of Clinical Chemistry transferase method using an AST kit and ALT kit (Wako, Osaka, Japan) by the Clinical Analyzer Model 7180 (Hitachi High-Technologies Co., Tokyo, Japan).

### In vivo bioluminescent imaging and luciferase assay

In order to examine the expression and distribution of the transgene after hydrodynamic injection, *in vivo* bioimaging was performed. Mice were injected with 20  $\mu$ g of pGL3 control vector or saline as a control, and 24 h after the injection, were anaesthetised with a mixture of ketamine and xylazine. D-luciferin (potassium salt; Biosynth, Staad, Switzerland) was injected into the peritoneal cavity of mice at 2 mg·kg<sup>-1</sup>. After 5 min, luciferase activity was detected from the ventral surface using a noninvasive bioimaging system (IVIS; Xenogen, Alameda, CA, USA) [13, 14].

Furthermore, to precisely quantify luciferase activity in individual organs, the liver (quadrate lobe), right lung, heart, kidney and spleen were excised from mice 24 h after the hydrodynamic gene transfer. 1 ml of Passive Lysis Buffer (Promega) was added to the organs and homogenised with a Polytron homogenizer (Kinematica, Littau, Switzerland).

Homogenates were frozen ( $-80^{\circ}\text{C}$ ) and thawed twice and then centrifuged for 10 min at  $13,000 \times g$  at  $4^{\circ}\text{C}$ . The total protein content of the supernatants was determined by the Bradford method with protein assay dye reagent (Bio-Rad, Hercules, CA, USA) with calibration using bovine serum albumin (Sigma-Aldrich). For the luciferase assay, 10  $\mu\text{L}$  of supernatant homogenate was mixed with 50  $\mu\text{L}$  of luciferase assay reagent II (Promega), and luciferase activity was measured by a luminometer (Lumat LB9507; Berthold Technologies, Bad Wildbad, Germany). The data were presented as the relative light units per total protein content.

#### Detection of Lac Z protein

For visual confirmation of the gene expression in each organ, 20  $\mu\text{g}$  of pCAGGS-Lac Z and the same dose of pCAGGS, as a control, were introduced. 48 h after the hydrodynamic injection, mice were sacrificed and each organ (liver and lung) was excised and fixed with a mixture of 0.2% (v/v) glutaraldehyde and 1% (v/v) formaldehyde for 1 h at  $4^{\circ}\text{C}$ , and the samples were then stained with  $1 \text{ mg} \cdot \text{mL}^{-1}$  of 5-bromo-4-chloro-3-indolyl- $\beta$ -D-galactopyranoside (X-gal; Sigma-Aldrich).

#### ST2-overexpressing mice

In order to prepare ST2-overexpressing mice, pCAGGS-mST2 was introduced by hydrodynamic injection, and pCAGGS was used as a control. Starting 12 h after the gene transfer, blood was collected from the tail vein and the concentration of plasma ST2 protein was confirmed. Concurrently, bronchoalveolar lavage fluid (BALF) and lung homogenate were prepared for examining the ST2 protein in the lung. Lavage was performed under deep anaesthesia with a lethal dose of pentobarbital, and the trachea was cannulated with an 18-gauge catheter. The lungs were inflated with 1 mL of cold sterile saline, the solution was slowly recovered and centrifuged at  $400 \times g$  for 10 min at  $4^{\circ}\text{C}$ , and the resultant supernatant was collected and analysed.  $\sim 0.8 \text{ mL}$  of BALF was consistently recovered, and therefore this amount was used to determine the content of ST2 protein in BALF. To obtain the lung homogenate, the remaining mice were anaesthetised, as described previously, and perfusion of pulmonary vessels with 5 mL saline was carried out *via* the right ventricle. The lungs were then excised and homogenised in 2 mL cold saline using a Polytron homogenizer (Kinematica) on ice. The resultant solution was centrifuged at  $9,000 \times g$  for 15 min at  $4^{\circ}\text{C}$ , and the supernatant was subjected to analysis. The concentrations of ST2 protein in plasma, BALF and lung homogenate were measured by ELISA.

#### mST2 ELISA

The mST2 ELISA system was originally constructed in our laboratory, as previously described [7]. Briefly, the bottom of a 96-well ELISA plate (Sumitomo Bakelite Co., Tokyo, Japan) was coated with rat monoclonal antibody against mouse T1/ST2 protein (MD Biosciences, Zurich, Switzerland) and samples were added and incubated for 1 h at room temperature. Next, rabbit anti-mST2 polyclonal antibody [12] and HRP against rabbit IgG (GE healthcare UK Ltd, Chalfont St Giles, UK) were added consecutively. Finally, O-phenylenediamine solution was used as substrate and optical density was measured at 450 nm with a microplate reader (Inter Medical, Tokyo, Japan).

#### Induction of bleomycin-induced lung injury

Mice were anaesthetised by intraperitoneal injection of pentobarbital ( $50 \text{ mg} \cdot \text{kg}^{-1}$ ), then 50  $\mu\text{L}$  of bleomycin (Nippon Kayaku Co., Tokyo, Japan) dissolved in sterile saline was administered intratracheally, as previously reported [15]. To determine the appropriate dosage of bleomycin, bleomycin was administered preliminarily at different doses, 2.5 and  $1 \text{ mg} \cdot \text{kg}^{-1}$  to mice. In the  $2.5 \text{ mg} \cdot \text{kg}^{-1}$ -injected group, body weight decreased rapidly, and almost all animals died between days 7–10. Conversely, in the  $1 \text{ mg} \cdot \text{kg}^{-1}$ -injected group, about half of the mice remained alive. Therefore, it was established that the optimal bleomycin dose for our purpose was  $1 \text{ mg} \cdot \text{kg}^{-1}$ .

In plasmid-introduced mice, at 24 h after gene transfer (pCAGGS and pCAGGS-mST2) to mice, blood was sampled from the tail vein and the level of ST2 protein was determined. After an additional 24 h, as controls, the same volume of saline or the same dose of bleomycin was administered to mice after hydrodynamic injection with the same volume of saline (6.3% of the total body weight) without plasmid vectors.

#### Reverse transcriptase-PCR analysis

Bleomycin-induced mRNA expression of several cytokines and mST2 was examined by reverse transcriptase (RT)-PCR analysis. Mice that had not undergone gene transfer were administered bleomycin intratracheally, and after 1, 3 or 7 days, the whole lungs were removed and immediately immersed in 1 mL of TRI reagent (Sigma-Aldrich). After homogenisation with a Polytron homogeniser (Kinematica), total RNA was extracted and purified according to the manufacturer's protocol. Contaminated genomic DNA was destroyed by DNase I (Takara, Shiga, Japan), and cDNAs were synthesised using moloney murine leukaemia virus RT (Invitrogen, Carlsbad, CA, USA). The nucleotide sequence of the primers used were as follows. mST2: (forward) 5'-GCGG-AGAATGGAACCAACTA-3', (reverse) 5'-CAATGTGTGAGG-GACTCC-3';  $\beta$ -actin: (forward) 5'-TGTCCCTGTATGCC-TCTGGTA-3', (reverse) 5'-ACTGTGTTGGCATAGAGGTC-3'; tumour necrosis factor (TNF)- $\alpha$ : (forward) 5'-CTGGCAGG-GGCCACCACGCTC-3', (reverse) 5'-CTCAGCGCTGAGTTG-GTCCCCCTTCTC-3'; IL-1 $\beta$ : (forward) 5'-GCTGCTCCAAA-CCTTTGAC-3', (reverse) 5'-AGGCCACAGGTATTTTGTGCG-3'; and IL-33: (forward) 5'-ATGAGACCTAGAATGAAGTATT-CCA-3', (reverse) 5'-TTAGATTTTCGAGAGCTTAAACATA-3'. 10  $\mu\text{L}$  of PCR products were developed by electrophoresis on 1% agarose gels, and the gels were stained with ethidium bromide.

#### Measurement of cytokines and albumin in BALF

After the treatment with bleomycin, the lungs were lavaged four times with 0.7 mL of cold PBS. After lavage, the total number of cells was immediately counted and the cell type was identified. For the determination of cell types, cells obtained through centrifugation in a cytopspin at  $120 \times g$  for 10 min were stained with Diff-Quick (Sysmax, Kobe, Japan). The remaining BALF was centrifuged at  $400 \times g$  for 10 min at  $4^{\circ}\text{C}$ , and the supernatant was analysed. The concentrations of cytokines (TNF- $\alpha$ , IL-1 $\beta$  and IL-6) in BALF were measured using ELISA kits (Biosource, Camarillo, CA, USA), and albumin concentration was measured by a turbidimetric

immunoassay using R-ALB-UR (Kyokuto Pharmaceutical Industrial Co., Tokyo, Japan). Bronchoalveolar lavage (BAL) was performed four times with 0.7 mL PBS, and ~2.5 mL was continually recovered in each case.

### Histology

Mice were sacrificed and pulmonary vessels were perfused with 5 mL of saline *via* the right ventricle. Then, after intratracheal injection of 1 mL of 10% (v/v) neutral formalin buffered with 0.2 M cacodylate solution (pH 7.4), the lungs were excised and post-fixed with the same fixative for 10 h and were embedded in paraffin. Sections were cut into 6- $\mu$ m thick slices, which were stained by haematoxylin and eosin (H&E) solution and Mallory-Azan.

To quantify the histological findings, the tissue volume density (TVD) was calculated using Scion Image software (Scion Corporation, Frederick, MD, USA), and the proportion of airspace consolidation and atelectasis to the total areas was obtained.

### Analysis of body weight loss and survival after bleomycin treatment

24 h after hydrodynamic gene transfer (pCAGGS and pCAGGS-mST2), bleomycin was administered intratracheally (1 mg·kg<sup>-1</sup>). Over 14 days following gene transfer, the mortalities and body weights in each group of mice were monitored.

### Statistical analysis

The data are presented as mean  $\pm$  SD. Statistical analyses were performed by an unpaired *t*-test (comparing two groups) or by ANOVA followed by the Tukey's test (comparing multiple groups), and survival analysis was performed using the Kaplan-Meier method. SPSS 11.0J (SPSS Inc., Chicago, IL, USA) was used for each statistical analysis. *p*-values <0.05 were considered statistically significant.

## RESULTS

### Hydrodynamic gene transfer

Hydrodynamic injection, a strategy used to transfer naked plasmid DNA into animals, was applied to obtain ST2-overexpressing mice. First, in order to confirm the overexpression of the transgene by hydrodynamic injection, we injected the pGL3 control vector into the mice, and observed the luciferase expression *in vivo* (fig. 1a). Luciferase expression was most prominent around the upper abdomen, and was significantly elevated at day 1. No specific signals were detected in the saline-injected mice.

Next, to confirm the transgene expression in each organ, several organs (the liver, lung, heart, kidney and spleen) were excised and the luminescence activity was measured after hydrodynamic gene transfer of the pGL3 control vector. Figure 1b and c demonstrate that the liver showed outstanding luminescence activity, and thus, the liver is the only target organ of this gene transfer method. The other organs from the pGL3-injected mice showed lower luminescence activity than the liver, but higher activity than that of control mice. Furthermore, to detect transgene expression visually, pCAGGS-LacZ was administered in the same manner, and the liver and lung were excised and stained with X-gal

solution. As shown in figure 1d, the liver was clearly stained blue; however, there was almost no detectable  $\beta$ -galactosidase expression in the lung (fig. 1e). This outcome corresponded to the results of the bioluminescent assay.

### Transient overexpression of mST2 protein

Before *in vivo* application, to confirm the production of mature mST2 protein from the constructed plasmid, pCAGGS and pCAGGS-mST2 were transferred into HEK 293T cells. The culture supernatant was collected for Western blotting. As shown in figure 2a, both the glycosylated mature form of ST2 (60–70 kDa) and the core peptide (37 kDa) obtained by digestion with *N*-glycosidase F were clearly detected. The results indicated that the mature ST2 protein was appropriately expressed and secreted from the cultured cells using our constructed plasmid.

We then carried out *in vivo* gene transfer into mice using hydrodynamic injection. First, we determined the appropriate amount of plasmid for obtaining the maximum plasma concentration of the ST2 protein. As shown in figure 2b, various amounts of plasmid vectors (10–100  $\mu$ g) were introduced, and the concentration of plasma ST2 protein increased significantly in accordance with the amount of plasmid administered. It reached a maximum level when 50  $\mu$ g of the plasmid was injected, but no significant increase was observed when the amount of plasmid was increased from 50 to 100  $\mu$ g. Therefore, the amount of the plasmid was fixed at 50  $\mu$ g for the subsequent *in vivo* experiments.

The time-kinetics of the introduced ST2 protein were examined next. As shown in figure 2c, the ST2 protein level in plasma attained a peak at ~12–24 h (18.1–27.6  $\mu$ g·mL<sup>-1</sup>) and gradually decreased until 21 days (4.07  $\mu$ g·mL<sup>-1</sup>). Empty vector-injected mice showed no increase in ST2 level from the beginning to the end of the trial, indicating that the injection of plasmids itself did not exert any influence on the endogenous ST2 level. For examination of the level of local ST2 protein in the lung, 1 mL of saline was injected intratracheally to obtain BALF, and almost constant recovery of 0.8 mL was obtained. The level of BALF ST2 protein was 10.81  $\pm$  3.31 ng·mL<sup>-1</sup>, as measured by ELISA, and therefore the BALF ST2 protein content was estimated at 8.65  $\pm$  2.65 ng·BALF<sup>-1</sup>. To collect lung homogenate, the lungs were excised and homogenised in 2 mL of saline. Since the concentration of ST2 protein was 23.57  $\pm$  12.72 ng·mL<sup>-1</sup>, the content of ST2 protein in lung homogenate was 47.14  $\pm$  25.43 ng (fig. 2d and e).

Since the hydrodynamic method has been known to cause liver damage, AST and ALT levels were monitored after the injection. In the current study, AST/ALT levels were elevated at day 1, but returned to the normal range by day 2. There were no significant time-course differences in the serum AST/ALT concentration between empty vector-introduced mice and ST2-overexpressing mice (fig. 2f and g).

### mRNA expression of pro-inflammatory cytokines, endogenous ST2 and IL-33 in bleomycin-induced lung injury

TNF- $\alpha$  and IL-1 $\beta$  are pro-inflammatory cytokines that have been reported to be upregulated immediately after bleomycin exposure, and to play principal roles in the exacerbation of

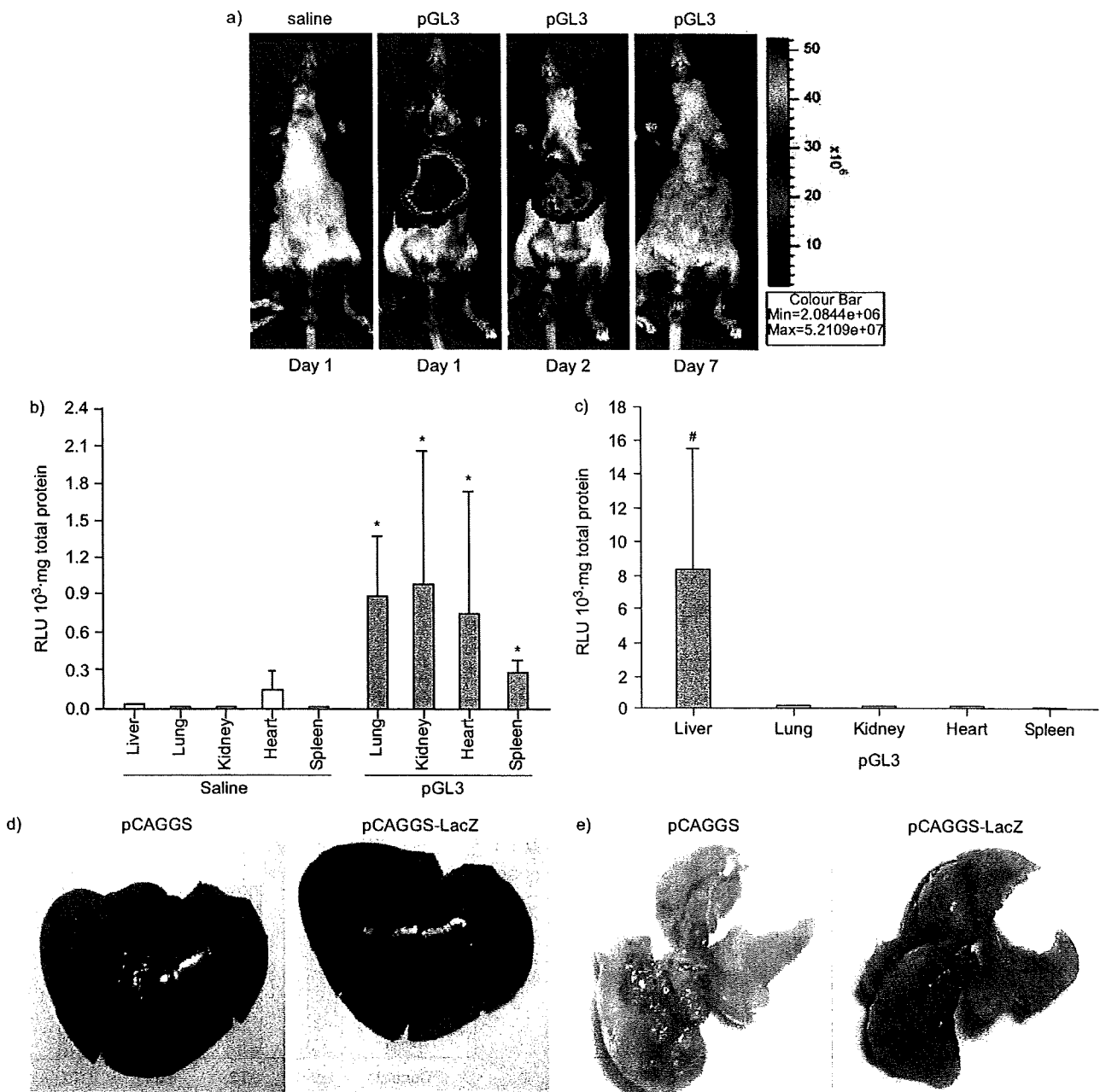


**FIGURE 1.** Detection of gene expression transferred by hydrodynamic injection. a) *In vivo* imaging of mice after the hydrodynamic injection of saline and pGL3 control vector. Luciferase expression was detected from the ventral surface of the body by IVIS (Xenogen, Alameda, CA, USA) for up to 7 days. The right panel indicates photon intensity correlating with the gene expression. The data are representative of four separate experiments showing similar results. b and c) *Ex vivo* luciferase assay of the individual organs. The luciferase activities of the liver, lung, heart, kidney and spleen at 24 h after the hydrodynamic injection of saline (control; □) and pGL3 control vector (■) were demonstrated as the relative light units (RLU) per total protein content. c) The luciferase activity of the liver was demonstrated independently using another scale. Data are presented as mean ± SD, n=4, and are representative of two independent experiments. \*: p<0.05; \*\*: p<0.01 versus relevant organ of saline injected group; #: p<0.01 versus other organs of pGL3-injected mice. General view of the left lobe of the liver (d), and right lobe of the lung (e) at 48 h after the hydrodynamic injection of pCAGGS or pCAGGS-LacZ. Each organ was excised and stained with 5-bromo-4-chloro-3-indolyl-β-D-galactopyranoside solution. Blue staining indicates the expression of β-galactosidase.

lung injury [16, 17]. In the present study, therefore, we examined the lung mRNA expression of the pro-inflammatory cytokines TNF-α and IL-1β after the intratracheal injection of bleomycin. As shown in figure 3, bleomycin treatment

remarkably increased the mRNA levels of TNF-α and IL-1β at day 1, demonstrating that acute lung injury occurred. The levels of both cytokines were decreased from day 3–7. We also examined the levels of lung endogenous ST2 and IL-33 mRNA,



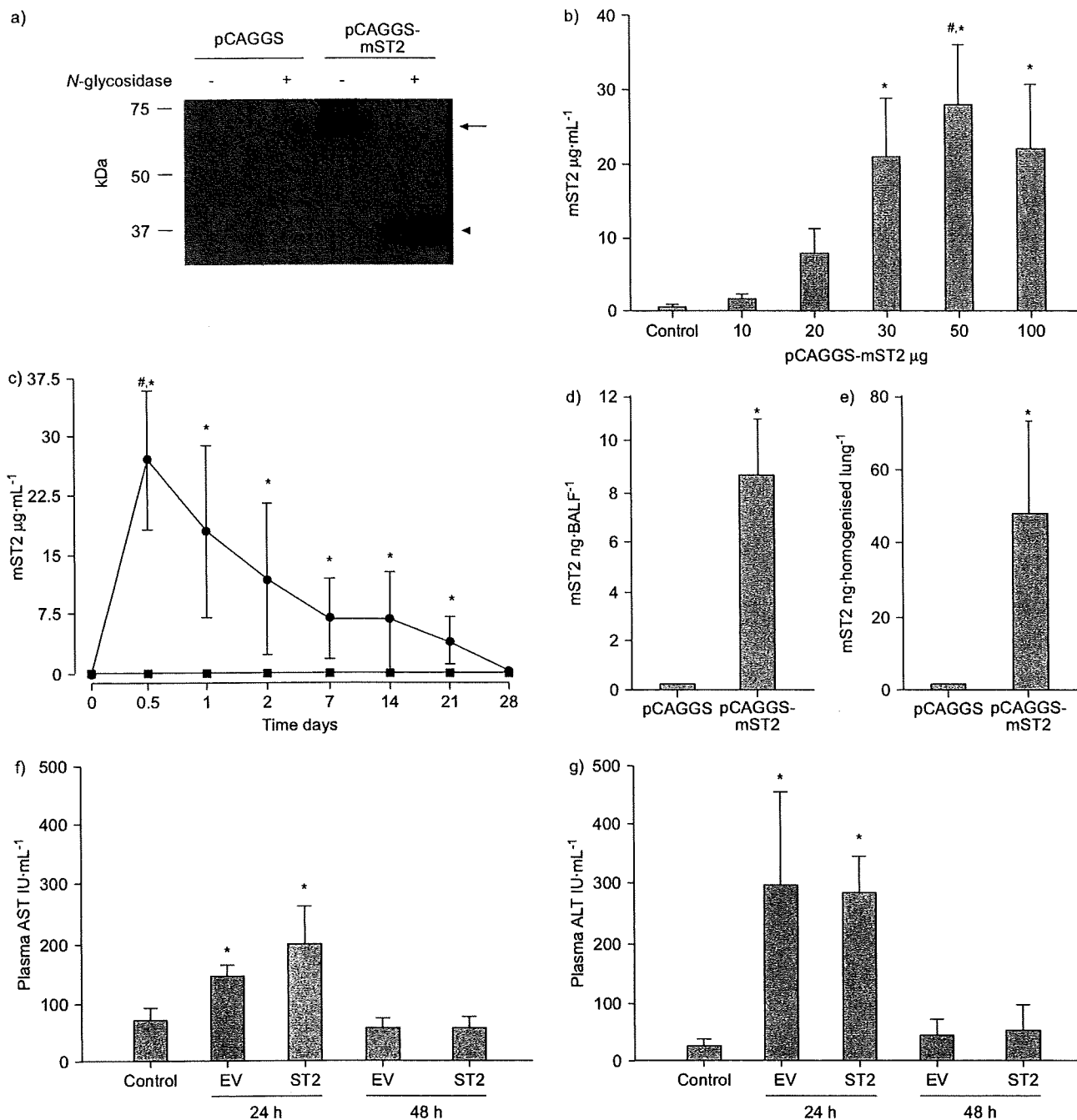


**FIGURE 2.** Assessment of ST2 gene transfer *in vitro* and *in vivo*. a) *In vitro* detection of mouse ST2 protein in the supernatants of human embryonic kidney (HEK) 293T cells after the gene transfer of pCAGGS and pCAGGS-mST2. These plasmid vectors were transferred by the calcium-phosphate method, and 24 h later, supernatants were collected and subjected to Western blotting. The presence of mature glycosylated ST2 protein (60–70 kDa; arrow) and deglycosylated core peptide (37 kDa; arrowhead) was confirmed. b) Concentration of plasma ST2 protein in mice injected with various amounts of plasmids. Mice were sacrificed at 12 h after the hydrodynamic injection of plasmid (pCAGGS-mST2) or same volume of saline (control), and the plasma was collected to measure the ST2 concentration. The data are presented as mean  $\pm$  SD, n=4, and are representative of three independent experiments. \*: p<0.05 compared with saline-injected mice; #: p<0.05 compared with other plasmid doses. c) Time kinetics of plasma ST2 protein after the hydrodynamic injection with 50 µg of plasmid. Mice were bled consecutively from the tail vein on each day, and plasma was prepared. The data are presented as the mean  $\pm$  SD, n=4, and are representative of three independent experiments. \*: p<0.05 pCAGGS-injected group versus pCAGGS-mST2-injected group at the same plasmid dose; #: p<0.05 compared with other timing in pCAGGS-mST2-injected group. ●: pCAGGS-mST2; ■: pCAGGS. d and e) ST2 protein in lung homogenate (d) and bronchoalveolar fluid (BALF; e) at 24 h after hydrodynamic injection. The data are presented as mean  $\pm$  SD, n=3, \*: p<0.05 compared with pCAGGS-injected mice. f and g) Serum aspartate aminotransferase (AST; f) and alanine aminotransferase (ALT; g) levels after the hydrodynamic gene transfer. The data are presented as the mean  $\pm$  SD, n=3, and are representative of two independent experiments. \*: p<0.05 compared with saline injected mice (without plasmid injection). EV: empty vector.

which were weakly and constitutively expressed without bleomycin treatment; however, these mRNAs gradually increased in a time-dependent manner from day 3 to day 7 after bleomycin treatment.

**Analysis of BALF cell counts and cell types after bleomycin administration**

To examine the acute extravasation of inflammatory cells into the pulmonary interstitium caused by bleomycin, BAL was performed at day 1 and day 3 after bleomycin treatment, and we analysed the total cell counts and cell types. Compared with the levels in control mice treated with saline, the total cell numbers and number of neutrophils were significantly elevated at day 1 in bleomycin-treated mice (fig. 4a and b).

We then examined whether the ST2 protein affected the initial inflammatory phase in acute lung injury, using bleomycin-treated ST2-overexpressing mice and mice injected with empty vector as controls. The time course is presented in figure 5. First, it was confirmed that the hydrodynamic injection itself did not affect the total cell count in the empty vector- and pCAGGS-ST2-injected mice (fig. 4a). In mice treated with empty vector plus bleomycin and mice treated with bleomycin alone, the total number of cells immediately increased on day 1. However, in ST2-overexpressing mice, the total cell number was significantly reduced compared with the other bleomycin-treated mice. Furthermore, in mice with empty vector plus bleomycin, numbers of neutrophils were prominently elevated at day 1. In contrast, a significant decrease in the number of neutrophils and lymphocytes was evident on day 1 in ST2-overexpressing mice (fig. 4b).

Conversely, on day 3, the total cell counts in ST2-overexpressing mice were estimated to be almost equivalent to those in mice treated with bleomycin alone, as well as empty vector-injected plus bleomycin-treated mice. However, even though there were no significant statistical differences, the counts of neutrophils were relatively low and the counts of

lymphocytes were high in ST2-overexpressing mice, compared with the other bleomycin-treated groups.

**Pro-inflammatory cytokines and albumin levels in BALF**

In the present study, total cell counts and neutrophils were particularly increased in the initial phase of bleomycin-induced lung injury. The concentrations of pro-inflammatory cytokines in BALF at day 1 after the bleomycin treatment were then assayed and compared between groups. In bleomycin-treated mice, significant increases of TNF- $\alpha$ , IL-1 $\beta$  (data not shown) and IL-6 were demonstrated, and levels were almost equivalent to or slightly lower than those in the mice treated with empty vector plus bleomycin. In ST2-overexpressing mice, the concentration of TNF- $\alpha$  was significantly reduced compared with that of mice injected with empty vector plus bleomycin or that of mice treated with bleomycin alone (fig. 6a). In addition, the level of IL-6 was also significantly decreased in ST2-overexpressing mice (fig. 6b). The level of IL-1 $\beta$  was slightly lower in ST2-overexpressing mice, but there were no statistically significant differences (data not shown).

The albumin concentration in BALF is frequently used as an indicator of pulmonary vascular permeability, especially in the case of acute lung injury. In fact, bleomycin treatment induced a significant increase in albumin levels in bleomycin-treated mice in the present study. However, in ST2-overexpressing mice, the albumin concentration was significantly lower than in other bleomycin-treated mice (fig. 6c).

**Histological examination of the effect of ST2 protein on bleomycin-induced lung injury**

The effect of the ST2 protein on acute phases of bleomycin-induced lung injury was investigated histologically (fig. 7a and b). Mice treated only with saline exhibited a small-scale interstitial oedema in the early phase (day 1), but no inflammatory cells were observed in the perivascular area at that time (fig. 7a). The impact of the hydrodynamic injection histologically was also examined; the plasmid injection itself did not affect the pulmonary architecture (fig. 7a). Conversely, both the mice treated with bleomycin alone and those treated with empty vector plus bleomycin showed an accumulation of inflammatory cells around the bronchovascular bundle, and in higher magnification, many neutrophils with segmented nuclei and some round mononuclear cells were recognised (fig. 7b). In contrast, rare inflammatory cells were observed in the peribronchial area in ST2-overexpressing mice, but accumulations of neutrophils were not observed (fig. 7a and b).

In general, following the inflammatory phase in bleomycin-induced lung injury, connective tissues and extracellular matrix are increased [17]. We performed Mallory-Azan and H&E staining of the lung tissue sections on day 7 after administration of bleomycin (fig. 8). Mice treated with saline alone and mice injected with plasmid vector alone had no inflammatory change and no alteration of the pulmonary architecture was observed (fig. 8a). However, a large number of inflammatory cells was observed in the mice treated with bleomycin alone and those treated with empty vector plus bleomycin; the infiltrating cells accumulated in the subpleural and peribronchial areas, and the airspaces showed wide-ranging collapse (fig. 8a). Furthermore, there was a large amount of blue-stained connective tissue throughout the alveolar interstitium, especially in the severely

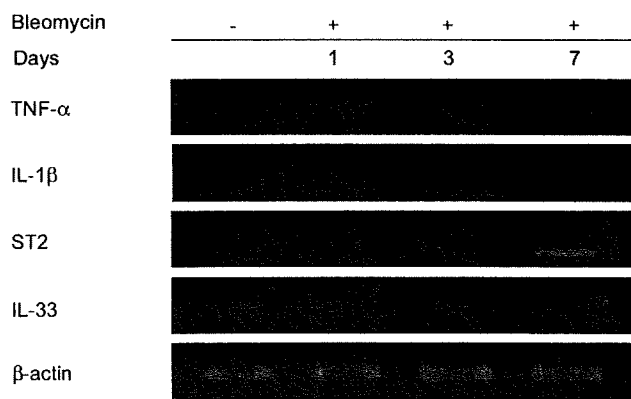


**FIGURE 3.** mRNA expression of pro-inflammatory cytokines, ST2 and interleukin (IL)-33 after bleomycin treatment. Bleomycin was administered intratracheally to wild-type mice at days 1, 3 and 7, after day 7 the whole lung was excised and each mRNA expression was assayed. Mice without bleomycin treatment were controls.  $\beta$ -actin was a house-keeping gene and provided endogenous control. Similar results were obtained in three separate experiments. TNF- $\alpha$ : tumour necrosis factor- $\alpha$ .

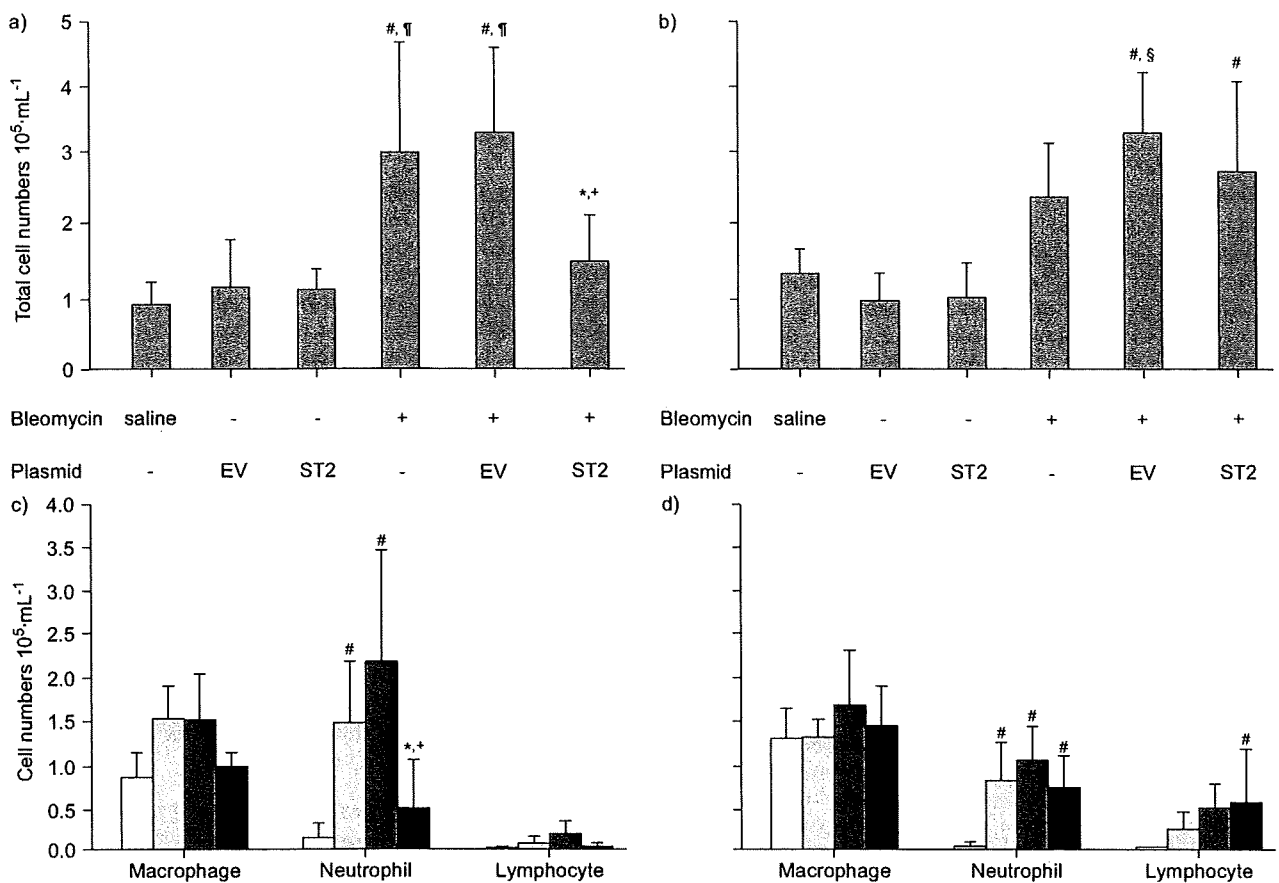


**FIGURE 4.** Analysis of total cell numbers and cell types in bronchoalveolar lavage fluid (BALF). BALF analysis was performed in mice with or without hydrodynamic gene transfer at day 1 (a and c) and day 3 (b and d) after the administration of bleomycin. a and b) Total cell numbers and c and d) cell types in BALF are shown. The data are presented as the mean  $\pm$  SD of four independent experiments. a and b) Saline: n=5; bleomycin: n=6; EV (empty vector; pCAGGS) or ST2 (pCAGGS-mST2): n=3; and EV or ST2 +bleomycin: n=10. c and d) Saline (□): n=5; bleomycin (○): n=6; and EV (■) or ST2+bleomycin (■): n=8. \*: p<0.05 ST2 plus bleomycin versus bleomycin alone; +: p<0.01 ST2 plus bleomycin versus EV plus bleomycin; #: p<0.01 compared with saline; ¶: p<0.01 compared with EV and ST2 (without bleomycin); §: p<0.05 compared with bleomycin alone.

damaged area (fig. 8b). Conversely, in ST2-overexpressing mice, some inflammatory cells were observed, but the areas of inflammation were restricted. Most of the alveolar structure

looked nearly normal, and it was clear that there was less connective tissue compared with other bleomycin-treated mice (fig. 8a and b).

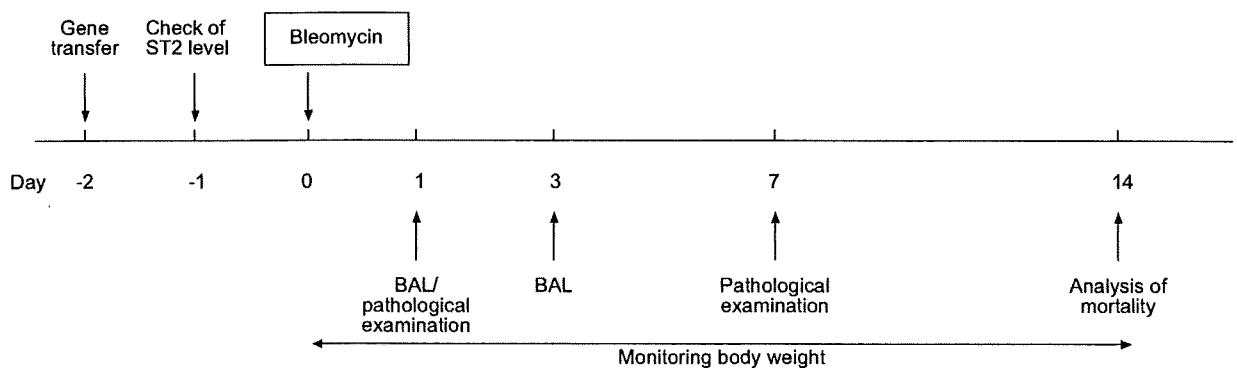


**FIGURE 5.** Time course of the experiments. The time course of the experiments to examine the effect of ST2 for the bleomycin-induced acute lung injury was presented schematically. The gene transfer was performed by the hydrodynamic injection of plasmids. BAL: bronchoalveolar lavage.

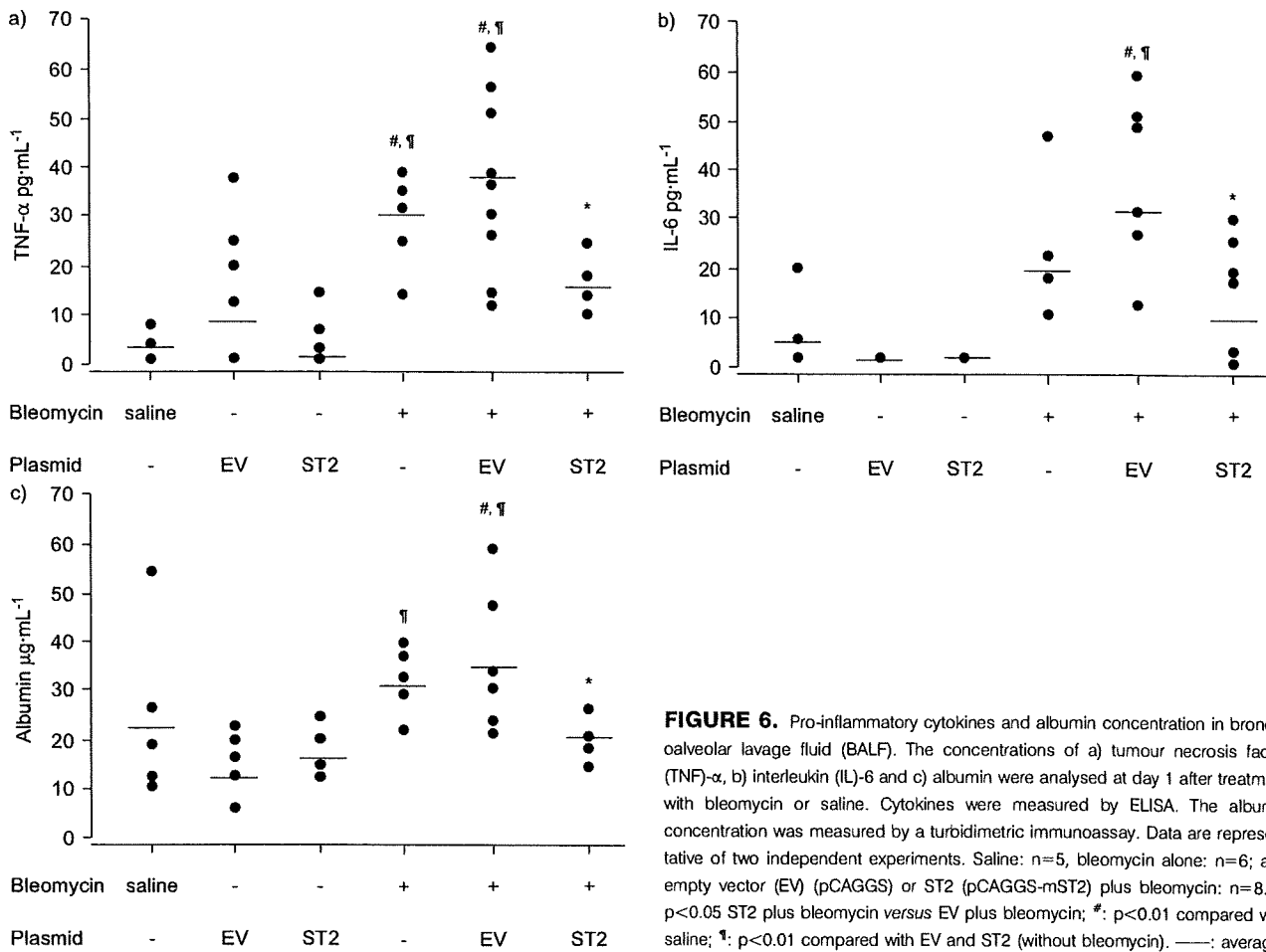


**FIGURE 6.** Pro-inflammatory cytokines and albumin concentration in bronchoalveolar lavage fluid (BALF). The concentrations of a) tumour necrosis factor (TNF)- $\alpha$ , b) interleukin (IL)-6 and c) albumin were analysed at day 1 after treatment with bleomycin or saline. Cytokines were measured by ELISA. The albumin concentration was measured by a turbidimetric immunoassay. Data are representative of two independent experiments. Saline: n=5, bleomycin alone: n=6; and empty vector (EV) (pCAGGS) or ST2 (pCAGGS-mST2) plus bleomycin: n=8. \*: p<0.05 ST2 plus bleomycin versus EV plus bleomycin; #: p<0.01 compared with saline; ¶: p<0.01 compared with EV and ST2 (without bleomycin). —: average.

Next, Scion Image software was used (Scion Corporation, Frederick, MD, USA) to quantify TVD to visualise the histological results at day 7 after bleomycin treatment. TVD was presented as the ratio of the collapsed high-density area to total area, and it increased in proportion to the extent of lung injury. Mice treated with bleomycin alone or treated with empty vector plus bleomycin showed significantly higher TVD than saline-treated mice. Conversely, in ST2-overexpressing mice treated with bleomycin, TVD was significantly lower than in other bleomycin-treated mice (fig. 8c).

**Body weight loss and survival rate in bleomycin-induced lung injury**

Body weight loss was monitored during the 14 days after bleomycin administration in ST2-overexpressing mice and empty vector-injected mice (fig. 9a). During the first week, most of the experimental mice remained alive, but their body weights decreased to varying degrees. In the second week, although the difference between the two groups was not statistically significant, the empty vector-injected mice continuously lost body weight, while the body weight of the ST2-overexpressing mice tended to remain constant.

Finally, we compared the survival rate for 14 days after bleomycin administration between ST2-overexpressing mice

and the other groups of mice (saline, bleomycin and empty vector plus bleomycin; fig. 9b). The survival rate of ST2-overexpressing mice was 84.0% at day 14 and the mean survival time was 13.44 days (95% confidence interval (CI) 12.92–13.96). The survival rates of mice treated with an empty vector plus bleomycin and bleomycin treatment alone were 43.5% and 63.6% and mean survival times were 11.7 (95% CI 10.58–12.81) and 12.2 days and (95% CI 10.76–13.60), respectively. ST2-overexpressing mice showed significantly higher survival rates than the other control groups. No mice died from hydrodynamic injection only (data not shown).

**DISCUSSION**

Some recent reports have suggested that the ST2 protein is induced by various inflammatory stimuli and may play an anti-inflammatory role *in vivo* [6–10]. TAJIMA and co-workers [8, 18] reported an increase of serum ST2 protein in acute exacerbation of idiopathic pulmonary fibrosis, and that ST2 gene expression was induced in the murine lung by intratracheal administration of bleomycin. Therefore, we speculated that ST2 was closely related to lung inflammation. We induced acute lung injury using bleomycin in the present study, and then assessed the effect of ST2 protein *in vivo*.